NASA TECHNICAL NOTE

NASA TN D-7392

NASA TN D-7392

RELIABILITY AND EFFECTIVE THERMAL CONDUCTIVITY OF THREE METALLIC-CERAMIC COMPOSITE INSULATING COATINGS ON COOLED HYDROGEN-OXYGEN ROCKETS

by Harold G. Price, Jr., Ralph L. Schacht, and Richard J. Quentmeyer

Lewis Research Center
Cleveland, Ohio 44135

NATIONAL AERONAUTICS AND SPACE ADMINISTRATION • WASHINGTON, D. C. • NOVEMBER 1973

1. Report No.	2. Government Accession No.	3. Recipient's Catalog No.
NASA TN D-7392		

4. Title and Subtitle	5. Report Date
RELIABILITY AND EFFECTIVE THERMAL CONDUCTIVITY OF THREE METALLIC-CERAMIC COMPOSITE INSULATING COATINGS ON COOLED HYDROGEN-OXYGEN ROCKETS	November 1973
	6. Performing Organization Code

7. Author(s)	8. Performing Organization Report No.
Harold G. Price, Jr., Ralph L. Schacht, and Richard J. Quentmeyer	E-7461
	10. Work Unit No. 502-24
9. Performing Organization Name and Address	11. Contract or Grant No.
Lewis Research Center National Aeronautics and Space Administration Cleveland, Ohio 44135	
	13. Type of Report and Period Covered Technical Note
12. Sponsoring Agency Name and Address	14. Sponsoring Agency Code
National Aeronautics and Space Administration Washington, D.C. 20546	

15. Supplementary Notes

16. Abstract

An experimental investigation of the structural integrity and effective thermal conductivity of three metallic-ceramic composite coatings was conducted. These coatings were plasma sprayed onto the combustion side of water-cooled, 12.7-centimeter (5-in.) throat diameter, hydrogen-oxygen rocket thrust chambers operating at 2.07 to 4.14 MN/m^2 (300 to 600 psia) chamber pressure. The metallic-ceramic composites functioned for six to 17 cycles and for as long as 213 seconds of rocket operations and could have probably provided their insulating properties for many additional cycles. The effective thermal conductivity of all the coatings was in the range of 0.7472 to 4.483 W/(m)(K) (0.1×10^{-4} to 0.6×10^{-4} Btu/(in.)(sec)(^{o}R)), which makes the coatings a very effective thermal barrier. Photomicrographic studies of cross-sectioned coolant tubes seem to indicate that the effective thermal conductivity of the coatings is controlled by contact resistance between the particles, as a result of the spraying process, and not the thermal conductivity of the bulk materials.

17. Key Words (Suggested by Author(s))	18. Distribution Statement
Heat transfer Hydrogen-oxygen rocket engines Metal and ceramic rocket coatings Nuclear rockets	Unclassified - unlimited

19. Security Classif. (of this report)	20. Security Classif. (of this page)	21. No. of Pages	22. Price*
Unclassified	Unclassified	50	Domestic, $3.00 Foreign, $5.50

* For sale by the National Technical Information Service, Springfield, Virginia 22151

RELIABILITY AND EFFECTIVE THERMAL CONDUCTIVITY OF THREE METALLIC-CERAMIC COMPOSITE INSULATING COATINGS ON COOLED HYDROGEN-OXYGEN ROCKETS

by Harold G. Price, Jr., Ralph L. Schacht, and Richard J. Quentmeyer

Lewis Research Center

SUMMARY

An experimental investigation of the structural integrity and effective thermal conductivity of three metallic-ceramic composite coatings was conducted at the Lewis Research Center. These coatings were plasma sprayed onto the combustion side of water-cooled, hydrogen-oxygen rocket thrust chambers.

The thrust chambers were operated over a chamber pressure range of 2.07 to 4.14 meganewtons per square meter (300 to 600 psia) with combustion maintained at 15 to 25 percent hydrogen fuel by weight (O/F of 5.67 to 3).

The first coating was a five-layer composite with molybdenum as the first layer on the wall. The molybdenum layer was followed by three layers, each varying in percent composition by weight (graded layers), of mixtures of molybdenum and zirconia. The final layer was a mixture of hafnia and zirconia. This coating functioned for 17 rocket firing cycles with a duration time of 213 seconds. A second composite coating with molybdenum as the first layer, three graded layers of mixtures of nichrome and alumina, and a fifth layer of 100-percent alumina functioned for six cycles with a duration time of 182 seconds. The third composite coating considered had a molybdenum first layer and nichrome and zirconia as the second and third layers, respectively. This coating also functioned for six cycles. The coatings were intact after the runs, and all the coatings could have probably survived many additional cycles.

The effective thermal conductivity of all the coatings was in the range of 0.7472 to 4.483 watts per meter per degree kelvin (0.1×10^{-4} to 0.6×10^{-4} Btu/(in.)(sec)(^{o}R)), which makes the coatings a very effective thermal barrier. Photomicrographic studies of cross-sectioned coolant tubes seem to indicate that the effective thermal conductivity of the coatings is controlled by contact resistance between the particles caused by the spraying process and not the thermal conductivity of the bulk materials.

INTRODUCTION

Coating the combustion side of a cooled rocket thrust chamber with a thermal insulation, if it can be done successfully, allows a rocket to operate at higher chamber pressures and combustion gas temperatures or at the same chamber pressure and temperature for more operating cycles (refs. 1 to 4). This is possible because the coating maintains or lowers the metal wall temperature, and also because the heat flux to the wall is reduced as the coating temperature goes up. Thus, there is a lower temperature differential across the metal coolant walls and lower metal thermal stresses.

In the past, coatings were usually made of single layers of ceramics sprayed onto metal. These ceramics are brittle materials, which have a tendency to spall and crack when subjected to the high heat-flux levels of a rocket combustion environment. The spalling and cracking result from high internal stresses caused by high temperature differentials which exist across the coating.

An alternative to the use of single-layer ceramic coatings is to build, upon the metal substrate, layers of coatings of varying thermal conductivity (graded coatings) to form a composite. In this manner, a gradual transition of thermal conductivity across the composite coating is formed, as opposed to the sharper transitions associated with single coatings. Thus, the temperature differential is more gradual and thermal stress may be reduced.

In reference 5, a number of graded coatings were tested in a small plasma rig. Four of these coatings that had the best structural integrity were further tested in reference 6 (heat-sink thrust chambers). Surprisingly, all of them gave about the same effective thermal conductivity. Photomicrographs seemed to indicate that contact resistance between the plasma-sprayed particles was the controlling factor in the effective thermal conductivity of the coatings.

In the present tests, three of the four coatings of reference 6 were applied to instrumented water-cooled 347-stainless-steel tubular rocket thrust chambers. These tests were run to establish the structural integrity of these coatings on cooled walls. The cooled rocket could be run for much longer times than the solid rocket used for the transient tests of reference 6. The coatings could also be subjected to many cycles of startup and shutdown to investigate the effect of extremes in operating conditions on coating adherence.

A further purpose of these tests was to determine the effective thermal conductivity of coatings plasma-sprayed onto cooled rocket thrust chamber walls. The thrust chambers used herein were instrumented to give the thermal performance of the coating under cooled rocket conditions. The cooled thrust chambers had the same internal dimensions as the copper heat-sink thrust chambers of reference 6. This thrust chamber shape has been studied extensively at the Lewis Research Center (refs. 7 and 8). The gas-side

heat-transfer correlations were determined and checked many times. These correlations are used in the present work.

The three different coatings were tested at the Rocket Engine Test Facility of the Lewis Research Center on three instrumented cooled rocket thrust chambers. The first coating (type 2) was a five-layer composite with molybdenum as the first layer on the tube wall. The molybdenum layer was followed by three layers, each varying in percent composition by weight (graded layers), of mixtures of molybdenum and zirconia. The final layer was a mixture of hafnia and zirconia. The second composite coating (type 3) had a molybdenum first layer, three graded layers of mixtures of nichrome and alumina, and a fifth layer of 100-percent alumina. The third composite coating (type 5) had a molybdenum first layer and nichrome and zirconia as the second and third layers, respectively.

Gaseous hydrogen and liquid oxygen were used as the propellants. A thrust of about 75 620 newtons (17 000 lbf) was developed at 4.14 meganewtons per square meter (600 psia) chamber pressure. The chamber pressure was varied between 2.07 and 4.14 meganewtons per square meter (300 and 600 psia), and combustion was maintained at 15-percent hydrogen fuel by weight (O/F of 5.67) with two tests at 25-percent hydrogen fuel by weight (O/F of 3).

APPARATUS

Thrust Chambers

Three water-cooled rocket thrust chambers were used to conduct the reliability and thermal conductivity experiments. The thrust chamber contour and dimensions are shown in figure 1. The contraction and expansion ratio of the nozzles was 4.64, and the characteristic length was 137.16 centimeters (54 in.). These cooled thrust chambers had the same internal geometry as the copper heat-sink thrust chambers of references 6 to 8. The cooling jacket was fabricated from 150 tubes of 347 stainless steel. Tubes with a wall thickness of 0.03048 centimeter (0.012 in.) were used in two of the thrust chambers, and the third chamber was fabricated from tubing with 0.0254-centimeter-(0.010-in.-) thick walls.

The geometric details, such as instrumentation station location, thrust-chamber diameter, and coolant channel height and chord width, are given in table I. A thrust of approximately 75 620 newtons (17 000 lbf) was developed at a chamber pressure of 4.14 meganewtons per square meter (600 psia) and a gas temperature of 3458 K (6224° R).

Coatings

Three of the coatings studied in reference 6 that had the best structural integrity were sprayed onto the combustion side of the rocket thrust chambers used in this investigation by means of a Plasmadyne SG-3, 25-kilowatt, 5.08-centimeter (2-in.) gun. The first coating tested (type 2) was a five-layer composite with molybdenum as the first layer on the wall. The molybdenum layer was followed by three layers, each varying in percent composition by weight (graded layers), of mixtures of molybdenum and zirconia. The final layer was a mixture of hafnia and zirconia. The second composite coating tested (type 3) had a molybdenum first layer, three graded layers of mixtures of nichrome and alumina, and a fifth layer of 100-percent alumina. The third composite coating tested (type 5) had a molybdenum first layer and nichrome and zirconia as the second and third layers, respectively.

To maintain a constant coating thickness, the spray angle was held perpendicular to the surface and the spray head was held a constant 5.08-centimeter (2-in.) distance from the surface during the spraying of the chamber to the throat section. The spraying facility did not have enough flexibility to maintain a constant coating thickness in the exit cone. The angle was kept perpendicular to the nozzle axis, but the distance from the surface increased as the gun traversed the exit cone. Thus coatings sprayed in the exit cone were not the same thickness as those sprayed in the throat section. An examination of table II shows the measured thickness of each of the coatings, as well as the composition details. The table also indicates the desired or design thicknesses to maintain a combustion-side wall temperature below the coating melting point and yet provide for a lower temperature drop across the metal tube wall.

The actual thicknesses were taken from photomicrographs (e.g., fig. 2) of the tube cross sections of an extra tube mounted in the thrust chamber during the spraying process. Coating thicknesses for the same coating on different thrust chambers also varied as shown in table II.

Injector

A coaxial injector, shown in figure 3, was used with liquid oxygen and gaseous hydrogen as the propellants. The injector had 234 elements uniformly spaced in a dish-shaped porous Rigimesh faceplate with an average of 0.4 element per square centimeter (2.6 elements/in.^{2}). Four to 6 percent of the gaseous hydrogen flowed through the faceplate at operating conditions of 2.07-meganewton-per-square-meter (300-psia) chamber pressure and 15-percent hydrogen fuel by weight (O/F of 5.67). One and one-half percent of the gaseous hydrogen propellant flowed through an outer ring of 72 peripheral film cooling holes of 0.066-centimeter (0.026-in.) diameter. The outer film cooling

flow of hydrogen was directed so that the jets of hydrogen impinged on the combustion-side wall 2.54 centimeters (1 in.) downstream from the injector face. This injector was the same as that used in reference 6.

Instrumentation and Data Recording

Two coolant tubes (circumferentially 180° apart) were used for instrumentation. Five axial stations were instrumented as shown in figure 4. The stations are also listed in table I. At each of these stations, five measurements were taken. Interface temperatures T_{uw} were obtained from two platinel/7674-stainless-steel thermocouples spot welded to the stainless-steel tube and plated over with nickel. Reference 9 is a detailed report of the installation of these miniaturized thermocouples. Two Chromel-constantan thermocouples were installed in the coolant passage, one 1.27 centimeters (0.5 in.) upstream and one 1.27 centimeters (0.5 in.) downstream of the interface thermocouple locations. A static pressure tap was installed on the coolant tube 0.762 centimeter (0.3 in.) upstream of the interface temperature measurement. These readings plus the pressures and temperatures measured at the inlet and outlet manifolds gave the water coolant pressure and temperature distributions through the passage. Three Chromel-constantan thermocouples were used in the inlet and four in the outlet manifolds. The instrumented thrust chamber is shown in figure 5.

Propellant flows, chamber pressures, coolant flows, interface temperatures, coolant pressures, and coolant temperatures were recorded in a digital form on a magnetic tape and also entered into the memory of an IBM 360 computer. The digital system used a sampling rate of 3125 words per second for 100 channels. Since the data were all steady state, 25 readings were averaged over an 0.8-second interval to eliminate 60-hertz noise and to diminish random noise. One report was made for all parameters at a common time. This report was then used in all terminal calculations, which were reported at the test site within minutes of the run. The times of the terminal calculations could be varied to best represent the steady-state conditions and to best keep track of any changes in the coatings.

TEST PROCEDURE

The rocket thrust chamber was installed on a test stand at the Lewis Rocket Engine Test Facility, as shown in figure 6. The facility was designed so that the water coolant flow rate and pressure could be controlled independently of the combustion flows of oxygen and hydrogen. Once the water coolant flow rate and pressure were established by preset valves, the propellant valves for controlling the gaseous hydrogen and liquid oxy-

gen were automatically ramped open by an electrical servocontroller to establish a preset combustion chamber pressure and the percent H_2 fuel by weight (O/F). The tests covered a chamber pressure operating range of 2.07 to 4.14 meganewtons per square meter (300 to 600 psia) with combustion varied from 15- to 25-percent H_2 by weight (O/F of 5.67 to 3). Table III summarizes the thrust chamber running conditions.

DATA ANALYSIS

The four basic equations that apply for a one-dimensional heat balance across a coated tube wall are

$$q = h_c(T_{cw} - T_c) \tag{1}$$

$$q = \left(\frac{k}{t}\right)_m (T_{uw} - T_{cw}) \tag{2}$$

$$q = \left(\frac{k}{t}\right)_{ct} (T_{gw} - T_{uw}) \tag{3}$$

$$q = h_g(T_{aw} - T_{gw}) \tag{4}$$

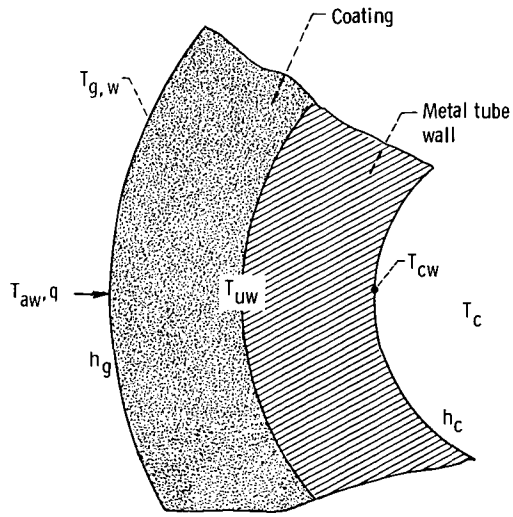

These equations can be used to analyze the heat transfer across the thrust chamber tube walls since the two-dimensional effects are minimized because the thrust chamber was constructed with thin-walled, low-thermal-conductivity stainless-steel tubes.

In order to solve for the effective thermal conductivity of the coating, an iterative procedure was employed that used the following measured parameters: T_c, T_{uw}, W_c, W_{H_2}, W_{O_2}, P_{ch}, $P_{s,c}$, t_m, and t_{ct}. All symbols are defined in appendix B. (The coating design analysis is presented in appendix A.)

The coolant-side heat-transfer coefficient h_c for water was obtained from the equation

$$(St^*)(Pr^*)^{0.6} = 0.019(Re^*)^{-0.2} \qquad \text{(ref. 10)} \tag{5}$$

The water properties were applied at the reference temperature T^* and static pressure $P_{s,c}$, where

$$T^* = \frac{T_s + T_{cw}}{2} \tag{6}$$

The static temperature T_s was calculated from an isentropic expansion through the thrust chamber.

The thermal conductivity of the type 347 stainless steel was evaluated at the mean temperature T_{mean} by the following equation, where k_m is in Btu/(in.)(sec)($^\circ$R) and T_{mean} is in $^\circ$R:

$$k_m = 1.17\times10^{-7}\, T_{mean} + 1.31\times10^{-4} \tag{7}$$

where

$$T_{mean} = \frac{T_{cw} + T_{uw}}{2} \tag{8}$$

which was fitted in the region of interest determined from reference 11. Equations (1) and (2) were then solved simultaneously for coolant wall temperature T_{cw} and heat flux q.

The hot-gas adiabatic wall temperature T_{aw} was computed by the method explained in reference 7 with the measured chamber pressure P_{ch} and propellant flow rates W_{H_2} and W_{O_2}.

The hot-gas-side heat-transfer coefficient h_g was computed from the correlation

$$(St^*)(Pr^*)^{0.7} = C_g\left(Re_d^*\right)^{-0.2} \tag{9}$$

obtained from reference 7. The hot-gas transport properties were put in as a function of static chamber pressure $P_{s,ch}$ and reference temperature T*. These hot-gas heat-transfer correlation coefficients C_g were developed for rocket thrust chambers having approximately a 1.63-micrometer rms (64-μin. rms) surface. The finishes of the coated thrust chamber tubes were measured to be 3.302 micrometers rms (130 μin. rms). Since this represents a small change in roughness, no corrections to the C_g were made. The axial measuring stations used in this report were identical with those used in reference 6. Equations (3) and (4) are solved simultaneously to get $(k/t)_{ct}$ and the gas-side wall temperature T_{gw}. Then, the coating thickness t_{ct} having been measured, the effective thermal conductivity of the coating k_{ct} can be computed.

DISCUSSION OF RESULTS

Reliability

All the coatings, in general, demonstrated good structural integrity, as shown in figure 7. However, the coating over the nickel(Ni)-plated region at the instrument stations did not survive as well as in the nonplated regions. This difference in structural integrity may be related to the method of fabrication. In this work, molybdenum (Mo) was used as the first layer in all the composite coatings tested. There is a considerable difference in the coefficient of thermal expansion between Ni and Mo. Also there is a possibility of comparatively rapid diffusion of Mo through the Ni, with the possible formation of brittle intermetallic compounds at the interface. Kvokova and Lainer in reference 12 suggest using a thin silver plating between the Mo and Ni to prevent the diffusion of the Mo into the Ni. This was attempted late in the program, but not enough testing was done to determine if it was successful.

Figure 8 shows the composite type 2 (thrust chamber 9) coating at axial station 6 after 17 runs. While the coating was in very bad condition over the Ni-plated areas, it was in excellent condition everywhere else. Coating type 2 functioned for 17 cycles and a total running time of 213 seconds with very minor damage. The damaged area over the instrumented stations was estimated to be less than 1 percent of the total coated surface area. The running was not continued, but the coating could have probably functioned for many more cycles.

Thrust chamber 8 (coated with type 3 coating) was the only thrust chamber cross sectioned after the testing, and photomicrographs showed the coating to have no significant erosion. The actual measurements indicated the coating had grown about 0.00508 centimeter (0.002 in.), but this is not probable. The final thickness could only be compared to the initial measurements from the extra tubes that were installed in the rocket thrust chamber during the coating process and then removed and cross-sectioned. The

original measurements showed a maximum variation of 28 percent in coating thickness between two tubes installed 180° apart in a thrust chamber during the coating process. The 0.00508-centimeter (0.002-in.) apparent growth falls in the tolerance of these measurements.

Coating types 3 and 5 functioned for six cycles and a total running time of 182 seconds. Again running was not continued because the coating thermal performance had been obtained and showed repeatibility between cycles.

Thermal Performance

Figure 9 is a plot of the measured interface temperature T_{uw} (between the tubes of 347 stainless steel and the coating) against accumulated running time and various operating conditions for composite coating type 2. Each data point is the averaged measured value for a steady-state condition where 25 readings have been averaged over an interval of 0.8 second. Each run was for 10 seconds, and it took from 0.2 to 0.3 second to reach steady-state conditions. Furthermore, each point is for a separate test; thus, the coating experienced a heat-up and cool-off cycle between each two points of data. The data are presented for five axial stations.

The thrust chamber had two tubes that were each instrumented with two T_{uw} thermocouples, and therefore four measurements were possible at each time report at each axial station. Because the thermocouple installation is a very precise and intricate process, no one engine was successfully instrumented with 40 T_{uw} thermocouples, that is, some were lost during the fabrication process. Others were lost during running, that is, the readings were invalid because of coating loss (fig. 8). And on some, the insulation cracked and new thermocouples were formed at other than the crown of the tube and thus gave erroneous readings. For these reasons, data are only plotted where repeated runs indicated a repeat of the measured quantities, T_{uw} and T_c, for a given running condition of P_{ch}, percent H_2, and W_c. When T_{uw} would not repeat, we found that usually the coating had been lost, which caused an increase in the reading of T_{uw}, or that the coating had separated from the metal, which caused a decrease in the reading of T_{uw}.

Since direct viewing of the coating after firing or viewing of photographs taken after firing did not always reveal any flaws (the coating could separate from the metal but still be intact), comparisons of T_{uw} were considered a better means of determining whether the coating (and thus the data) was still good. This was especially true in view of the fact that, for each of the coatings, more than one station could be found where T_{uw} did remain constant for many reruns where operating conditions were repeated.

Figure 9 shows that the measured values of T_{uw} are reasonably repeatable, which indicates that there was no coating deterioration. For example, at the approximate

times of 20, 30, 40, 50, and 60 seconds, the running conditions were repeated (as noted in the legend) and the measurements of T_{uw}'s were nearly the same. The measurements at about 10 and 70 seconds also indicate approximately the same values of T_{uw} for the same running condition. At some axial stations, a 55.6 K (100° R) difference is shown between the measurements on two tubes at the same axial station. An example of this is at a time of about 90 seconds at stations 4 and 9, which are just downstream of the throat. These differences could have a number of causes. The coolant flow could be slightly different in the two tubes. The plating thickness over the thermocouples themselves could be slightly different. Or the coating thickness from one side of the engine to the other could have varied.

Figure 10 is a plot of the coating effective thermal conductivity k_{ct} as a function of accumulated running time and operating condition computed using the average location interface temperature measurements of figure 9. This plot shows that the effective thermal conductivity varies little for many runs at the same operating condition. The data indicate that the effective thermal conductivity is not a strong function of percent fuel and only a slight function of chamber pressure.

The spread of the data is somewhat large but typical of results from actual rocket firings. The 55.6 K (100° R) difference in T_{uw} on opposite tubes gives about a 2-to-1 variation in thermal conductivity at stations 4 and 9. Sensitivity of k_{ct} to T_{uw} is discussed later, in the section Data Sensitivity.

Figure 11 is a plot of interface temperature for this same coating repeated on another thrust chamber. This plot, along with figure 12, which is a plot of k_{ct} against accumulated time, shows the same trends as figures 9 and 10.

Figure 13 is a plot of the interface temperature T_{uw} as a function of accumulated running time and operating condition for coating composite type 3. The type 2 coating was removed from this thrust chamber by blasting with number 60 aluminum oxide (Al_2O_3) grit. The thrust chamber was then recoated. Again, the measurements of T_{uw} are fairly repeatable over many cycles.

Figure 14 is a plot of k_{ct} against accumulated running time for coating composite type 3. At station 4 the value of k_{ct} was 1.868 watts per meter per kelvin (0.25×10^{-4} Btu/(in.)(sec)($^{\circ}$R)), which is approximately the same as for type 2. At stations 1, 2, and 5 the value of k_{ct} for type 3 was lower than for type 2.

Figures 15 and 16 are the same types of plots (T_{uw} and k_{ct} against time) for layered coating type 5. Again, the data are fairly repeatable over many cycles. The value of the effective thermal conductivity is also of the order of 2.242 watts per meter per kelvin (0.3×10^{-4} Btu/(in.)(sec)($^{\circ}$R)), which is about the same as for types 2 and 3. Reference 6 found a value of 2.989 watts per meter per kelvin (0.4×10^{-4} Btu/(in.)(sec)($^{\circ}$R)) to be representative of these three coating systems. In general, the present results substantiate the findings of reference 6, where the effective thermal conductivities of the coating were found not to be a function of chamber pressure or percent

fuel and only slightly affected by the average coating temperature. Similarly, as in reference 6, the thermal conductivity of the bulk materials used in the coatings also does not seem to have a great effect on the effective thermal conductivity of the composites. For example, adding a metal to the ceramic did not change the effective thermal conductivity of the overall coating. Apparently, contact resistance and resistances caused by interparticle bonds have a greater determining effect on the effective thermal conductivity of the plasma-sprayed system as applied than does the thermal conductivity of the bulk materials used in making up the composite.

The data of figures 9 to 16 are summarized in figures 17 to 19. The data points are the averages from the many runs obtained under similar operating conditions. The hot-gas wall temperature T_{gw} at the throat is approximately 1944 K (3500° R), which is probably approaching the limiting temperature for composites with alumina.

Figure 18 is a plot of the heat flux q against axial location in the thrust chamber relative to the throat computed using averaged measured temperatures of figure 17. Figure 19 is a plot of the effective thermal conductivity k_{ct} against axial location for the same conditions as figures 17 and 18. These effective thermal conductivities thus represent the averages for many runs for composite type 2 coating. The change in k_{ct} level with axial distance must be attributed to the way the coating was applied, as described in the section APPARATUS, Coatings. This undoubtedly changed the contact resistance of the system and thus k_{ct}. The k_{ct} variation at any one station represents the difference between three operating conditions and the different results for the same coating applied to two different thrust chambers. The k_{ct} varies from 1.12 to 3.74 watts per meter per kelvin (0.15×10^{-4} to 0.50×10^{-4} Btu/(in.)(sec)(°R)) in the region of the thrust chamber where spraying parameters were best controlled.

Figure 20 is a plot of k_{ct}, as obtained from the averaged T_{uw} measurements, for the three different coating types against the thrust chamber axial location at 4.14-meganewton-per-square-meter (600-psia) chamber pressure. The majority of the data is located between 1.12 and 3.74 watts per meter per kelvin (0.15×10^{-4} and 0.50×10^{-4} Btu/(in.)(sec)(°R)). However, the data for stations 1, 2, and 5 for thrust chamber 8 with type 3 coating do not lie in the same range. They do, however, lie within the accuracy shown by a sensitivity study which is discussed in the following section, Data Sensitivity.

Although there is no ready explanation for the discrepancy in the coating type 3 data at stations 1, 2, and 5, these were the only data obtained from a recoated thrust chamber. There is the possibility that the number 60 Al_2O_3 blasting of the thrust chamber, which was done to remove the coating type 2, could have affected the thermocouples at these stations.

The effective thermal conductivities found by the present data are approximately the same as those found in reference 6, which again lends credence to the data being good up to the point of separation or to the point where the coating was lost.

Data Sensitivity

In order to determine the accuracy of the effective thermal conductivities obtained, the C_g's, T_{uw}'s, and combustion efficiencies η from the data were perturbed. For example, the C_g's from reference 7 were perturbed from C_g to $C_g \pm 1.96\ \sigma$, where σ is the standard deviation of the C_g's from reference 7. Table IV shows the effect at the chamber and throat for a typical test. The table shows that k_{ct} and the gas-side wall temperature T_{gw} are very sensitive to perturbations of C_g (also shown graphically in appendix A). A perturbation of $1.96\ \sigma$ caused a 4-to-1 change in the k_{ct} value obtained for the chamber, and a 1.7-to-1 change for the throat. The changes in T_{gw} were 1.9 to 1 in the chamber and 1.4 to 1 at the throat. A designer will have to be conservative in his design procedure in the use of coatings, or more elaborate laboratory measurements will have to be made to determine the value of k_{ct} more accurately. A designer will also have to know the value of the hot-gas-side heat-transfer coefficient, probably from measurements instead of using a correlation.

The measurement of T_{uw} was perturbed by -55.6 K (-100° R), which was about the maximum variation obtained from two interface thermocouples at the same position. In general, the experimental variation was much less than 55.6 K (100° R). This variation is probably caused by thermocouple installation location error, plating thickness variation, and/or thermocouple error. The results are given in table V. The perturbation of T_{uw} by -55.6 K (-100° R) again produces large variations in k_{ct} and T_{gw}. Looking at the situation in reverse, the data show that a 7-to-1 variation in k_{ct} will not cause large changes in the interface temperature T_{uw}. The designer will again have to be conservative in the coating (gas-side wall) temperature T_{gw} he designs for.

Perturbations of the coolant adiabatic wall temperature T_c and of the coolant weight flow W_c had little effect on the value of k_{ct}. This is shown graphically in appendix A.

Perturbations of combustion efficiency gave the results shown in table VI. The table shows that a 2.7 percent drop in efficiency caused a 48 and 33 percent change in k_{ct} at the chamber and throat, respectively. The gas-side wall temperature T_{gw} for the 2.7 percent change in efficiency resulted in a 21 and 17 percent change at the chamber and throat, respectively.

Thickness measurements on two tubes inserted 180° apart in a thrust chamber during the coating process showed that the coating thickness varied by 28 percent. This 28 percent maximum variation in thickness would, of course, cause a 28 percent variation in the k_{ct} values.

Thus, small variations in the data can cause large changes in the value of the effective thermal conductivity and of the coating temperature obtained. This range of data scatter is reasonable since the data are within the range of most other thermal conductivity measurements on the materials used herein that are given in the literature.

Theoretical Coating Advantages

In order to show the advantages of a coating, six computer calculations were made. Three calculations each were performed for a coated thrust chamber and an uncoated thrust chamber. The calculations were performed for chamber pressures of 2.07, 3.10, and 4.14 meganewtons per square meter (300, 450, and 600 psia). The coating assumed was type 2 with a thickness of 0.0254 centimeter (0.010 in.) held constant throughout the thrust chamber. The value of effective thermal conductivity k_{ct} used was 2.24 watts per meter per kelvin (0.3×10^{-4} Btu/(in.)(sec)(^{o}R)). Thus, these calculations were for the same range and operating conditions as those of figures 17 to 20. Figures 21 to 23 show the results of these theoretical calculations. Figure 21 shows that the metal wall temperature for the highest operating conditions and at the most critical region, just upstream of the throat, decreased from a T_{gw} of 861 K (1550^{o} R) for the uncoated chamber to a T_{uw} of 656 K (1180^{o} R) for the coated chamber by the use of the thermal barrier coating. Remember that $T_{uw} = T_{gw}$ for an uncoated thrust chamber. It also shows that the metal wall surface temperature with a thermal barrier is less sensitive to change in operating conditions. At the throat for the uncoated case, T_{uw} varies from 678 to 861 K (1220^{o} to 1550^{o} R), while for the coated case, T_{uw} varies from 583 to 656 K (1050^{o} to 1180^{o} R) for a change in chamber pressure from 2.07 to 4.14 meganewtons per square meter (300 to 600 psia). Figure 21(b) also shows that T_{gw} (or the coating surface temperature), 2347 K (4225^{o} R), just upstream of the throat is probably approaching the limiting temperature for zirconia for the highest chamber pressure.

Figure 22 shows very significant reductions in q by the application of a thermal barrier coating at the highest operating condition. Just upstream of the throat, q changed from 27.5 to 15.0 megawatts per square meter (16.8 to 9.2 Btu/(in.^{2})(sec)).

Figure 23 is a plot of ΔT across the metal wall with and without a thermal barrier coating. At the highest operating condition and just upstream of the throat, ΔT varied from 422 to 256 K (760^{o} to 460^{o} R). Thus, not only the absolute magnitude of the metal surface temperature was reduced, but also the ΔT across the metal was drastically reduced. These two factors should do much for increasing the life of a thrust chamber.

SUMMARY OF RESULTS

An experimental investigation was conducted at the Lewis Research Center with instrumented water-cooled thrust chambers. These thrust chambers were coated with three different coatings and were tested at chamber pressures of 2.07 to 4.14 meganewtons per square meter (300 to 600 psia) with hydrogen and oxygen as the propellants. The proportion of fuel was maintained at 15-percent hydrogen by weight (O/F of 5.67) with two tests at 25-percent hydrogen by weight (O/F of 3).

The results of the investigation are as follows:

1. The coatings, while not sprayed optimally, did perform repeatably and did function for many cycles over 99 percent of the thrust chamber.

2. Coating type 2 (a graded series of zirconia and molybdenum layers with a hafnia and zirconia outer layer) functioned for 17 cycles and a total running time of 213 seconds with very minor damage (less than 1 percent). The test was not continued, but after inspection of the coating it was determined to have a high probability of functioning many more cycles.

3. Coating type 3 (a graded series of alumina and nichrome layers with molybdenum underlayer) and type 5 (a layered molybdenum-nichrome-zirconia coating) each functioned for six cycles and a total running time of 182 seconds. The test was not continued, but after inspection of the coating it was determined to have a high probability of functioning many more cycles.

4. The effective thermal conductivity is not a function of pressure, average ceramic temperature, or percent hydrogen in the fuel (O/F) in the range of variables covered by these tests and with the accuracy obtainable by actual rocket firings.

5. The various coatings tested herein are very effective thermal barriers, with little difference in their effectiveness.

6. The effective thermal conductivity of the coatings was measured to be approximately 0.7472 to 4.483 watts per meter per kelvin (0.1×10^{-4} to 0.6×10^{-4} Btu/(in.)(sec)(^{o}R)), which is approximately equal to the thermal conductivity of the pure ceramic alone.

7. Contact resistance between the coating particles and layers is the controlling factor, and not the thermal conductivities of the bulk materials.

Lewis Research Center,
National Aeronautics and Space Administration,
Cleveland, Ohio, June 7, 1973,
502-24.

APPENDIX A

COATING DESIGN ANALYSIS

This appendix shows, through a series of graphical representations, how a designer can take the pertinent equations and a set of given input conditions, build up a set of plots which show the relative sensitivity of the input parameters, and establish a design envelope for coatings. Later in the appendix numerical examples are presented.

Reference 13 shows mathematically that for the case where a thin thermal shield, such as a refractory coating, is applied to a rocket thrust chamber, the thermal shielding reduces the heat-transfer coefficient to the shielded material to an effective value,

$$h_{eff} = \frac{h_g}{1 + h_g\left(\frac{t}{k}\right)_{ct}} \tag{1}$$

where h_g is the heat-transfer coefficient without the coating, t_{ct} is the coating thickness, and k_{ct} is the coating effective thermal conductivity. In figure 24(a) a graphical representation of equation (1) is shown for various values of $(t/k)_{ct}$. It can be seen that for large values of $(t/k)_{ct}$, h_{eff} is relatively insensitive to a wide variation in h_g. Thus, injector streaking or inability to accurately predict h_g would not adversely affect a design.

By taking the equation for one-dimensional heat flow to a coated wall

$$q = h_{eff}(T_{aw} - T_{uw}) = h_{eff}T_{uw}\left(\frac{T_{aw}}{T_{uw}} - 1\right) \tag{2}$$

where q is the heat flux per unit area, T_{aw} the adiabatic wall temperature, and T_{uw} the interface temperature between the coating and the metal wall, lines of constant q can be added to the graph in figure 24(a) for given values of T_{uw} and T_{aw}/T_{uw}. These are shown in figure 24(b). Since q is directly proportional to h_{eff} for given values of T_{uw} and T_{aw}/T_{uw}, it can be seen that the q lines are a linear progression on the h_{eff} axis with q equal to zero at h_{eff} equals zero.

The equation

$$q = h_g(T_{aw} - T_{gw}) \tag{3}$$

where T_{gw} is the gas-side wall temperature, can be combined with equation (2) to obtain

$$h_{eff} = h_g \left(\frac{\frac{T_{aw}}{T_{uw}} - \frac{T_{gw}}{T_{uw}}}{\frac{T_{aw}}{T_{uw}} - 1} \right) \tag{4}$$

By using equation (4), lines of constant T_{gw} can be added to the graph of h_{eff} against h_g for given values of T_{aw}/T_{uw} and T_{gw}. These lines are shown in figure 24(c) as a percentage of T_{aw}. The line $(t/k)_{ct} = 0$ is also a line of $T_{gw} = T_{uw}$, and the h_g-axis represents a line of $T_{gw} = T_{aw}$. Thus, having constructed the graph of figure 24(c) from a given set of input conditions, a designer has all the necessary information to establish a design envelope for coatings.

Figure 24(d) shows the sensitivity of the T_{gw} lines to various ratios of T_{aw}/T_{uw} for $T_{gw} = 0.5\ T_{aw}$. In this case ratios of T_{aw}/T_{uw} of 3.5 and 5.0 are shown. For a given T_{aw}, it can be seen that a maximum ratio of T_{aw}/T_{uw}, or minimum T_{uw}, is desirable since this shifts the T_{gw} lines to lower values of h_{eff} where the $(t/k)_{ct}$ lines flatten out. Besides the previous comments as to why one should design to be on the flat part of the $(t/k)_{ct}$ curves, this also allows a given design to operate over a much larger range of h_g.

In order to show the sensitivity of the various parameters shown in figure 24(d), a numerical plot has been constructed and shown in figure 24(e). In order to make an explanation of the sensitivity of the parameters used in figure 24(e) somewhat simpler, figures 25 to 27 were constructed. Figure 25 is for a T_{aw} of 2361 K (4250° R), which might be considered to be representative of a nuclear thrust chamber design. Figure 26 is for a T_{aw} of 3333 K (6000° R), which might be representative of a chemical rocket design with low chamber pressure or low q levels. Figure 27 is for a T_{aw} of 3611 K (6500° R), which might be representative of a chemical rocket design with high chamber pressure or high q levels. On all three plots, a k_{ct} of 2.242 watts per meter per kelvin (0.3×10^{-4} Btu/(in.)(sec)(°R)) and a T_{uw} of 556 K (1000° R) were used. This is representative of k_{ct} for all the coatings tested. Gas-side wall temperature T_{gw} lines of 1667, 1944, and 2222 K (3000°, 3500°, and 4000° R) and others have also been constructed for these plots.

The design should be in a region on these curves where the thickness curves have become horizontal so that, even though h_g changed, h_{eff} would remain the same. For example, using figure 25, a typical uncoated nuclear nozzle design might be at a q level of about 32.7 megawatts per square meter (20 Btu/(in.^{2})(sec)) (point A) and an h_g of 1.809×10^4 watts per square meter per kelvin (0.00615 Btu/(in.^{2})(sec)(°R)). By using a coating with a k_{ct} value of 2.242 watts per meter per kelvin (0.3×10^{-4} Btu/(in.)(sec)(°R)) and a thickness of approximately 0.0414 centimeter (0.0163 in.), the q level would be dropped to about 7.52 megawatts per square meter (4.6 Btu/(in.^{2})(sec))

with a T_{gw} of 1944 K (3500° R) (point B). In this region h_{eff} changes very slowly as h_g increases. Figure 26 with a driving temperature T_{aw} of 3333 K (6000° R) shows that for the same gas-side wall temperature, the same k, the same T_{uw}, and the same q as the uncoated case (point C), the thickness required would be about 0.01905 centimeter (0.0075 in.) and the q level would be dropped to 16.34 megawatts per square meter (10 Btu/(in.^{2})(sec)) (point D). One would like the design to be in the region where t_{ct} lines are horizontal, but the restraint is the upper temperature limit of the coating. Again using figure 27 where T_{aw} = 3611 K (6500° R), with the higher q's, for example 131 megawatts per square meter (80 Btu/(in.^{2})(sec)) uncoated (point E), 0.00437 centimeter (0.00172 in.) of coating would give a coating temperature of 1944 K (3500° R) and an assumed interface temperature T_{uw} of 556 K (1000° R) for a k_{ct} of 2.242 watts per meter per kelvin (0.3×10^{-4} Btu/(in.)(sec)(°R)) (point F).

Since contact resistance seems to be the major factor in establishing the effective thermal conductivity, spraying 0.00152 centimeter (0.00063 in.) of an oxide layer on copper for the future shuttle engines could reduce the q from 131 to 101 megawatts per square meter (80 to 62 Btu/(in.^{2})(sec)) (point G). This is predicated on the spraying of the oxide effectively to give a k_{ct} of 2.242 watts per meter per kelvin (0.3×10^{-4} Btu/(in.)(sec)(°R)). The gas-side wall temperature would only be about 1244 K (2239° R).

These examples show that a designer can easily draw up similar curves for his own design conditions (T_{aw} and T_{uw}) and then add T_{gw} lines for the temperature his coating can withstand. He then can pick thickness levels for a number of axial positions for his thrust chamber and immediately know the effectiveness and the q levels that go with these choices.

Figure 28 is a plot of the equation

$$\frac{T_{cw}}{T_{uw}} = \frac{1 + \left[\frac{h_c}{(k/t)_m}\right]\left(\frac{T_c}{T_{uw}}\right)}{1 + \frac{h_c}{(k/t)_m}} \tag{5}$$

which is the solution of the two basic equations

$$q = h_c(T_{cw} - T_c) \tag{6}$$

$$q = \left(\frac{k}{t}\right)_m (T_{uw} - T_{cw}) \tag{7}$$

This figure shows that in the flat region of the T_c/T_{uw} curves, T_{cw}/T_{uw} does not vary much with big changes in the parameter $h_c/(k/t)_m$.

Figure 29 is a graphical representation of the equation

$$\frac{T_{cw}}{T_{uw}} = \frac{1 + \left[\frac{h_g}{(k/t)_{ct}}\right]\left(\frac{T_{aw}}{T_{uw}}\right)}{1 + \frac{h_g}{(k/t)_{ct}}} \tag{8}$$

which is a solution of the two equations

$$q = h_g(T_{aw} - T_{gw}) \tag{3}$$

$$q = \left(\frac{k}{t}\right)_{ct} (T_{gw} - T_{uw}) \tag{9}$$

This figure shows that for small ratios of T_{aw}/T_{uw}, T_{gw}/T_{uw} is not very sensitive to changes in $h_g/(k/t)_{ct}$. For large ratios T_{gw}/T_{uw} becomes very sensitive to changes in $h_g/(k/t)_{ct}$.

In general then, the sensitivity of the various design parameters depends on the regions of these plots that the designer finds himself in for his particular design. Thus, a few graphical plots easily give an insight to coatings for a given design.

APPENDIX B

SYMBOLS

B	constant
C	constant
C_g	hot-gas heat-transfer correlation coefficient
c_p	specific heat
D	diameter
h	heat-transfer coefficient
k	thermal conductivity
P	pressure
Pr	Prandtl number, $c_p\mu/k$
q	heat flux
Re	Reynolds number, $\rho VD/\mu$
Re_d	Reynolds number based on diameter
St	Stanton number, $h_c/\rho^* V c_p^*$
T	temperature
ΔT	temperature difference
t	thickness
V	velocity
W	weight flow rate
η	combustion efficiency
μ	viscosity
ρ	density
σ	standard deviation

Subscripts:

aw	adiabatic wall
c	coolant (water)
ch	chamber
ct	coating

cw	coolant wall
d	diameter
eff	effective
g	gas
gw	gas-side wall
H_2	gaseous hydrogen
m	metal
mean	mean
O_2	liquid oxygen
s	static
uw	interface between metal and coating
x	reference

Superscript:

*	reference condition

REFERENCES

1. Hjelm, Lawrence N.; and Bornhorst, Bernard R.: Development of Improved Ceramic Coatings to Increase the Life of XLR 99 Thrust Chamber. Research-Airplane-Committee Report on Conference on the Progress of the X-15 Project. NASA TM X-57072, 1961, pp. 227-253.
2. Stubbs, V. R.: Development of a Thermal Barrier Coating for Use on a Water-Cooled Nozzle of a Solid Propellant Rocket Motor. Aerojet-General Corp. (NASA CR-72549), May 3, 1969.
3. Robbins, William H.; Bachkin, Daniel; and Medeiros, Arthur A.: An Analysis of Nuclear-Rocket Nozzle Cooling. NASA TN D-482, 1960, p. 11.
4. Curren, Arthur N.; Price, Harold G., Jr.; and Douglass, Howard W.: Analysis of Effects of Rocket-Engine Design Parameters on Regenerative-Cooling Capabilities of Several Propellants. NASA TN D-66, 1959.
5. Curren, Arthur N.; Grisaffe, Salvatore J.; and Wycoff, Kurt C.: Hydrogen Plasma Tests of Some Insulating Coating Systems for the Nuclear Rocket Thrust Chamber. NASA TM X-2461, 1972.
6. Schacht, Ralph L.; Price, Harold G., Jr.; and Quentmeyer, Richard J.: Effective Thermal Conductivities of Four Metal-Ceramic Composite Coatings in Hydrogen-Oxygen Rocket Firings. NASA TN D-7055, 1972.
7. Schacht, Ralph L.; Quentmeyer, Richard J.; and Jones, William L.: Experimental Investigation of Hot-Gas Side Heat-Transfer Rates for a Hydrogen-Oxygen Rocket. NASA TN D-2832, 1965.
8. Schacht, Ralph L.; and Quentmeyer, Richard J.: Axial and Circumferential Variations of Hot-Gas-Side Heat-Transfer Rates in a Hydrogen-Oxygen Rocket. NASA TN D-6396, 1971.
9. Huff, Ronald G.: A Thermocouple Technique for Measuring Hot-Gas-Side Wall Temperatures in Rocket Engines. NASA TN D-5291, 1969.
10. Swenson, H. S.; Carver, J. R.; and Kakarala, C. R.: Heat Transfer to Supercritical Water in Smooth-Bore Tubes. Paper 64-WA/HT-25, ASME, 1964.
11. Sachs, G.; and Pray, R. Ford, III, eds.: Air Weapons Materials Application Handbook. Metals and Alloys. Syracuse Univ. Research Inst. (ARDC-TR-59-66), Dec. 1959.
12. Toropov, N. A., ed.: Heat-Resistance Coatings. Consultants Bureau Enterprises, Inc., 1967.
13. Lin, C. C., ed.: Turbulent Flows and Heat Transfer. Vol. V of High Speed Aerodynamics and Jet Propulsion. Princeton Univ. Press, 1959.

TABLE I. - GEOMETRIC DESIGN DETAILS OF THRUST CHAMBER

AND COOLANT CHANNELS

Station	Axial location relative to throat (a)		Thrust-chamber diameter		Coolant-channel height perpendicular to flow[b]		Coolant-channel chord width[b]	
	cm	in.	cm	in.	cm	in.	cm	in.
Nozzle	26.817	10.558	26.632	10.485	0.457	0.180	0.564	0.222
5-10	20.386	8.026	23.178	9.125	.442	.174	.490	.193
----------	12.685	4.994	19.050	7.500	.406	.160	.401	.158
4-9	3.175	1.250	13.952	5.493	.330	.130	.292	.115
Tangent point	1.643	.647	13.132	5.170	.323	.127	.277	.109
----------	.820	.323	12.807	5.042	.320	.126	.269	.106
3-8 (throat)	0	0	12.700	5.000	.318	.125	.267	.105
----------	-1.643	-.647	13.132	5.170	.323	.127	.277	.109
Tangent point	-3.175	-1.250	14.402	5.670	.356	.140	.302	.119
2-7	-5.398	-2.125	16.967	6.680	.424	.167	.358	.141
Tangent point	-7.605	-2.994	19.530	7.689	.485	.191	.411	.162
----------	-12.220	-4.811	23.833	9.383	.572	.225	.505	.199
----------	-17.137	-6.747	26.469	10.421	.622	.245	.561	.221
1-6 (tangent point)	-22.210	-8.744	27.356	10.770	.638	.251	.579	.228
----------	-29.528	-11.625	27.356	10.770	.665	.262	.579	.228
----------	-35.278	-13.889	27.356	10.770	.688	.271	.579	.228

[a]Positive values denote locations downstream of throat; negative values denote locations upstream of throat.

[b]See fig. 4 (section B).

TABLE II. - COATING COMPOSITION AND THICKNESS

Thrust chamber	Coating type	Coating material composition, percent by weight	Design thickness per layer (constant thickness throughout thrust chamber)		Station									
					1-6		2-7		3-8		4-9		5-10	
					Total measured thickness									
			cm	in.	cm	in.	cm	in.	cm	in.	cm	in.	cm	in.
8	2	Mo	0.005	0.002	-------	-------	-------	-------	-------	-------	-------	-------	-------	-------
		83Mo-17ZrO_2	.005	.002	-------	-------	-------	-------	-------	-------	-------	-------	-------	-------
		63Mo-37ZrO_2	.005	.002	-------	-------	-------	-------	-------	-------	-------	-------	-------	-------
		36Mo-65ZrO_2	.005	.002	-------	-------	-------	-------	-------	-------	-------	-------	-------	-------
		64HfO_2-36ZrO_2	.010	.004	-------	-------	-------	-------	-------	-------	-------	-------	-------	-------
			0.030	0.012	0.02225	0.00876	0.02494	0.00982	0.02654	0.01045	0.01979	0.00779	0.01925	0.00758
9	2	Mo	0.005	0.002	-------	-------	-------	-------	-------	-------	-------	-------	-------	-------
		83Mo-17ZrO_2	.005	.002	-------	-------	-------	-------	-------	-------	-------	-------	-------	-------
		63Mo-37ZrO_2	.005	.002	-------	-------	-------	-------	-------	-------	-------	-------	-------	-------
		36Mo-65ZrO_2	.005	.002	-------	-------	-------	-------	-------	-------	-------	-------	-------	-------
		64HfO_2-36ZrO_2	.010	.004	-------	-------	-------	-------	-------	-------	-------	-------	-------	-------
			0.030	0.012	0.02794	0.0110	0.02642	0.0104	0.02304	0.00907	0.02390	0.00941	0.02550	0.01004
8	3	Mo	0.005	0.002	-------	-------	-------	-------	-------	-------	-------	-------	-------	-------
		70 Nichrome-30Al_2O_3	.005	.002	-------	-------	-------	-------	-------	-------	-------	-------	-------	-------
		30 Nichrome-70Al_2O_3	.005	.002	-------	-------	-------	-------	-------	-------	-------	-------	-------	-------
		10 Nichrome-90Al_2O_3	.005	.002	-------	-------	-------	-------	-------	-------	-------	-------	-------	-------
		100Al_2O_3	.010	.004	-------	-------	-------	-------	-------	-------	-------	-------	-------	-------
			0.030	0.012	0.01328	0.00523	0.01090	0.00429	0.01313	0.00517	0.01232	0.00485	0.00983	0.00387
5	5	Mo	0.005	0.002	-------	-------	-------	-------	-------	-------	-------	-------	-------	-------
		Nichrome	.008	.003	-------	-------	-------	-------	-------	-------	-------	-------	-------	-------
		ZrO_2	.010	.004	-------	-------	-------	-------	-------	-------	-------	-------	-------	-------
			0.023	0.009	0.02797	0.01101	0.02319	0.00913	0.02657	0.01046	0.02731	0.01075	0.02377	0.00936

TABLE III. - OPERATING CONDITIONS FOR TEST RUNS

Thrust chamber	Coating type	Throat coating thickness		Heat flux				Chamber pressure		Hydrogen content, percent by weight	Oxidant-to-fuel ratio	Effective thermal conductivity		Number of cycles	Total running time, sec
				Coated		Uncoated									
		cm	in.	W/m^2	$Btu/(in.^2)(sec)$	W/m^2	$Btu/(in.^2)(sec)$	N/m^2	psia			$W/(m)(K)$	$Btu/(in.)(sec)(^{\circ}R)$		
8	2	0.02654	0.01045	8.171×10^6 to 11.44×10^6	5 to 7	14.71×10^6 to 19.61×10^6	9 to 12	2.068×10^6 to 3.103×10^6	300 to 450	15 and 25	5.67 and 3.00	1.121 to 5.604	0.15×10^{-4} to 0.75×10^{-4}	12	115
9	2	.02304	.00907	10.62×10^6 to 15.53×10^6	6.5 to 9.5	14.71×10^6 to 24.51×10^6	9 to 15	2.068×10^6 to 4.137×10^6	300 and 600	15	5.67	1.121 to 5.604	0.15×10^{-4} to 0.75×10^{-4}	17	213
8	3	.01313	.00517	13.07×10^6	8	24.51×10^6	15	4.137×10^6	600	15	5.67	0.747 to 2.615	0.1×10^{-4} to 0.35×10^{-4}	6	182
5	5	.02657	.01046	11.44×10^6	7	24.51×10^6	15	4.137×10^6	600	15	5.67	0.747 to 2.615	0.1×10^{-4} to 0.35×10^{-4}	6	182

TABLE IV. - DATA SENSITIVITY - PERTURBATIONS IN HOT-GAS HEAT-TRANSFER CORRELATION COEFFICIENT

	Hot-gas-side wall temperature, T_{gw}		Coating effective thermal conductivity, k_{ct}	
	K	^{o}R	W/(m)(K)	Btu/(in.)(sec)(^{o}R)
Chamber				
$C_g = 0.0257$	1043	1878	1.7	0.23×10^{-4}
$C_g - 1.96\,\sigma = 0.0201$	680	1224	4.8	.64
$C_g + 1.96\,\sigma = 0.0313$	1294	2330	1.2	.16
Throat				
$C_g = 0.0151$	1513	2755	1.6	0.21×10^{-4}
$C_g - 1.96\,\sigma = 0.0112$	1211	2180	2.2	.29
$C_g + 1.96\,\sigma = 0.0190$	1731	3115	1.3	.17

TABLE V. - DATA SENSITIVITY - PERTURBATION IN INTERFACE TEMPERATURE

Interface temperature, T_{uw}		Hot-gas-side wall temperature, T_{gw}		Coating effective thermal conductivity, k_{ct}	
K	^{o}R	K	^{o}R	W/(m)(K)	Btu/(in.)(sec)(^{o}R)
Chamber					
522	940	1491	2683	6.8	0.91×10^{-4}
467	840	1157	2083	1.0	.14
Throat					
553	995	1957	3523	3.3	0.44×10^{-4}
497	895	1549	2788	1.3	.17

TABLE VI. - DATA SENSITIVITY - PERTURBATIONS

IN COMBUSTION EFFICIENCY

Combustion efficiency, η	Hot-gas-side wall temperature, T_{gw}		Coating effective thermal conductivity, k_{ct}	
	K	^{o}R	W/(m)(K)	Btu/(in.)(sec)(^{o}R)
Chamber				
0.984	1611	2900	2.1	0.28×10^{-4}
.970	1424	2563	2.5	.34
.957	1278	2301	3.1	.41
Throat				
0.984	2136	3845	2.1	0.28×10^{-4}
.970	1946	3502	2.4	.32
.957	1781	3206	2.8	.37

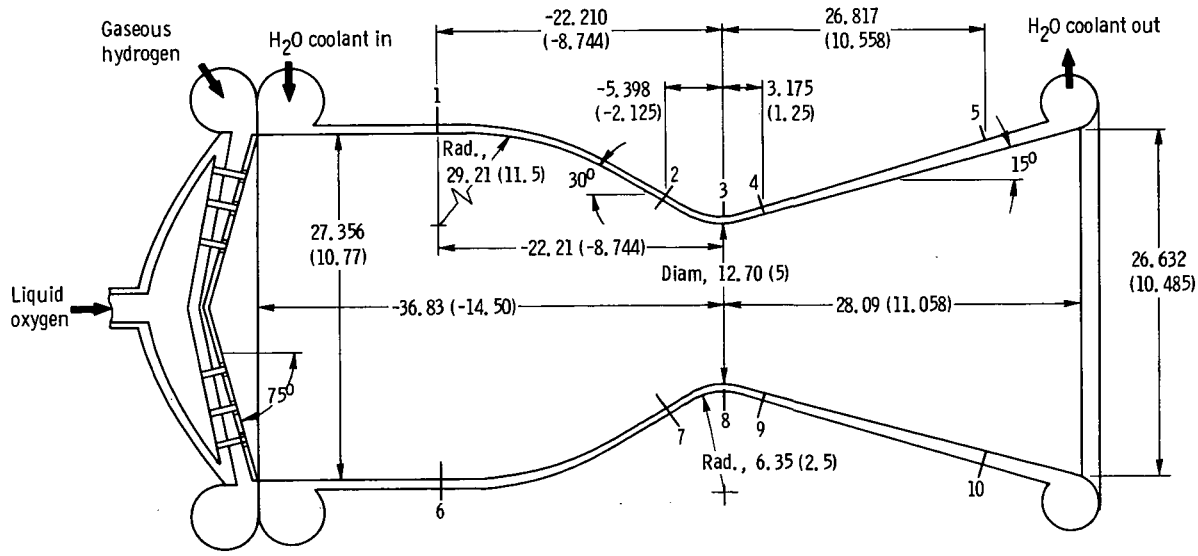

Figure 1. - Schematic of water-cooled rocket thrust chamber with coaxial injector. Contraction ratio, 4.64; expansion ratio, 4.64. (All linear dimensions are in centimeters (in.).)

Order of layers (all stations):

All ceramic

Mixed ceramic and metal

Metal sublayer

Parent tube material

Station 1

Station	Measured thickness[a]	
	mm	in.
1 (Chamber)	0.223	0.00876
2	.249	.00982
3 (Throat)	.265	.01045
4	.198	.00779
5 (Near exit)	.193	.00758

[a]Design thickness for all stations, 0.3048 mm (0.012 in.)

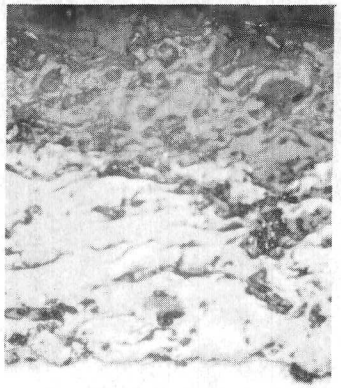

Station 2

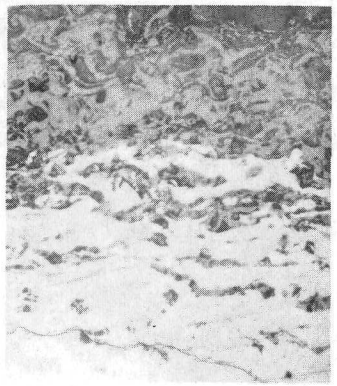

Station 3

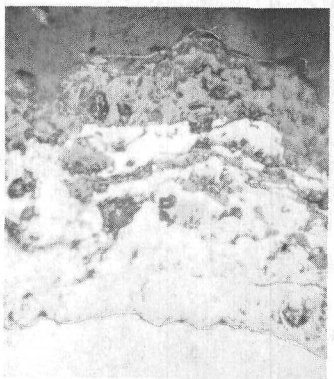

Station 4

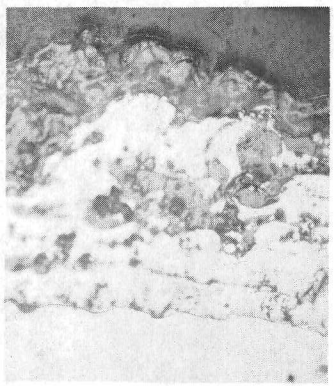

Station 5

Figure 2. - Typical photomicrographs of cross-sectioned tube, showing type 2 coating. X350.

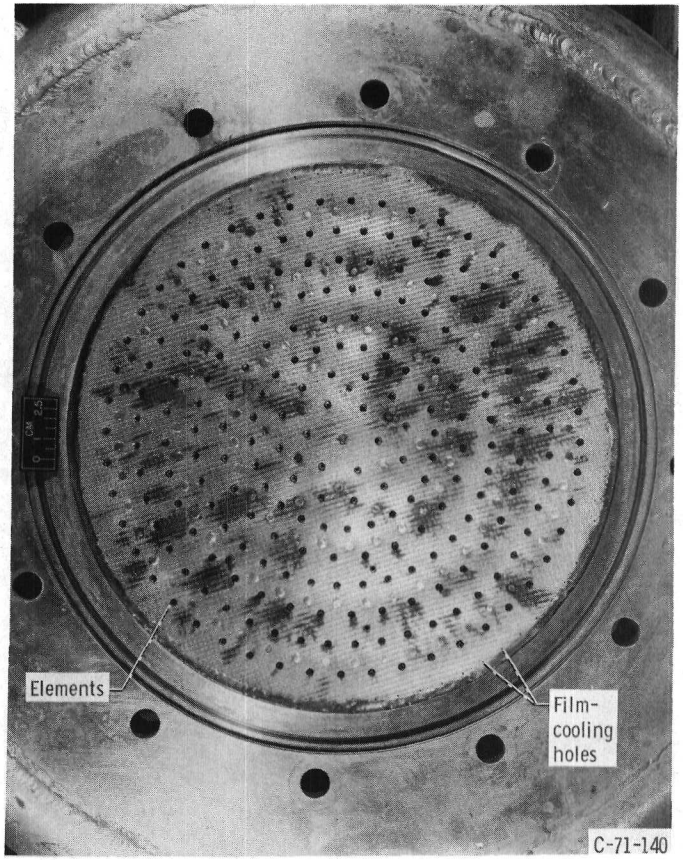

Figure 3. - Concentric tube injector with Rigimesh face.

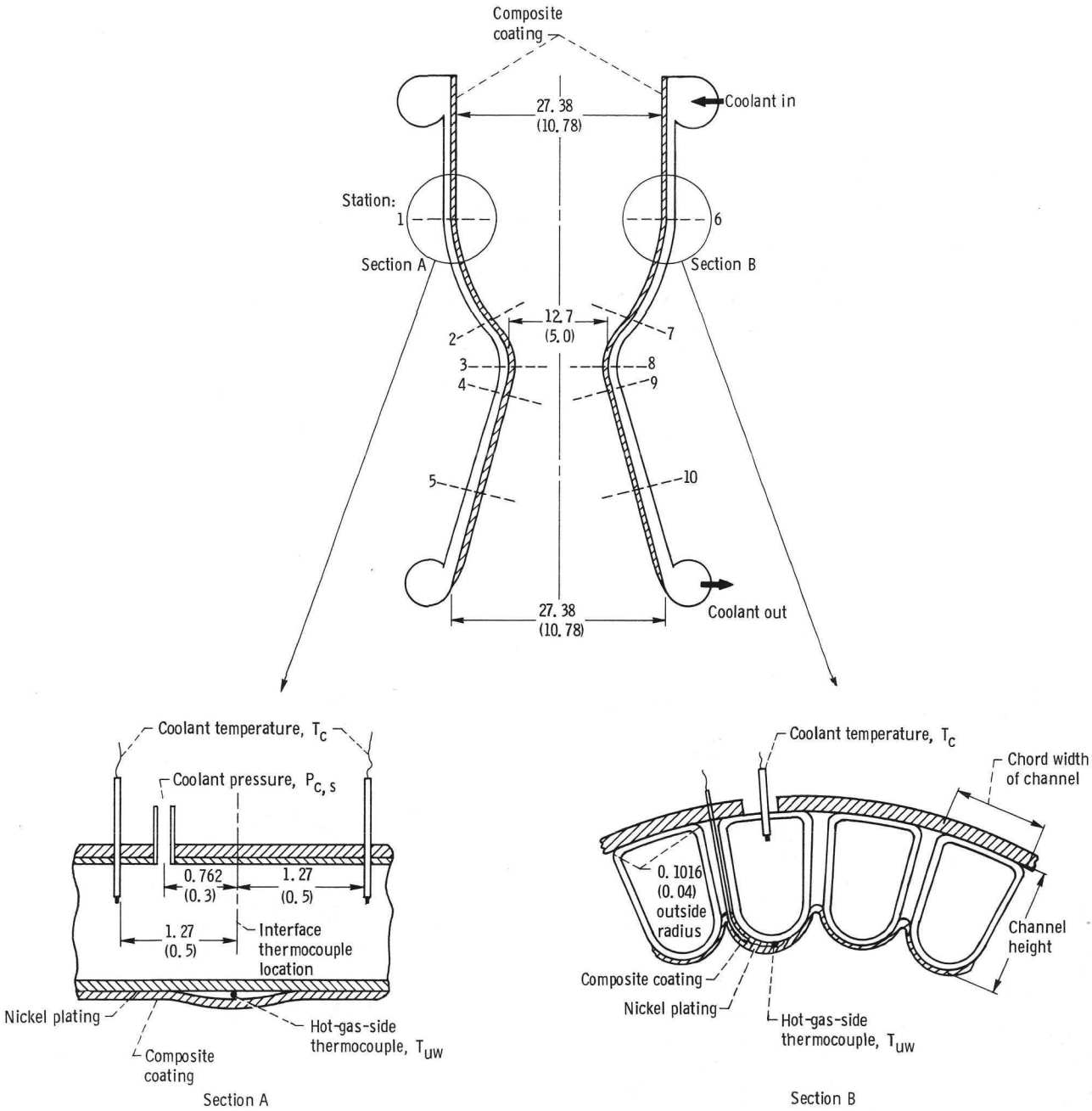

Figure 4. - Schematic of wire-wrapped water-cooled-nozzle instrumentation locations. Instrumentation at each station: coolant side, two Chromel-constantan thermocouples and one static-pressure tap; hot-gas side, two platinel - 7674-stainless-steel thermocouples. (All linear dimensions are in centimeters (in.).)

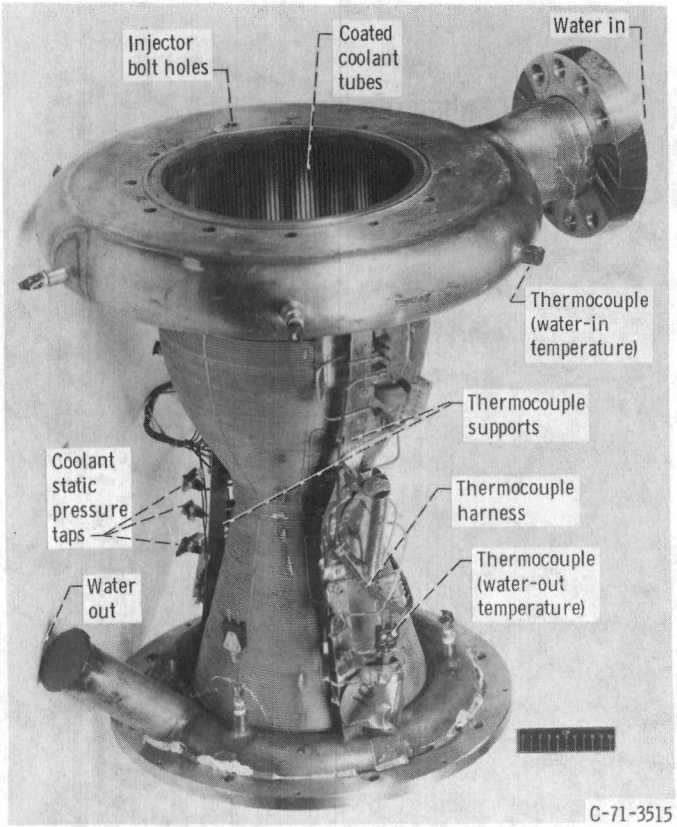

Figure 5. - Thrust chamber.

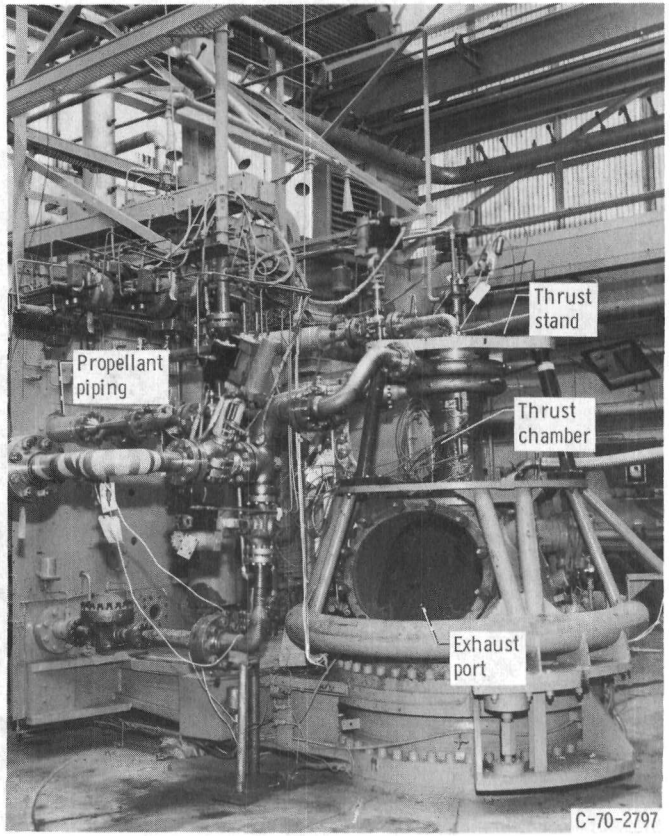

Figure 6. - Thrust chamber installed in test facility.

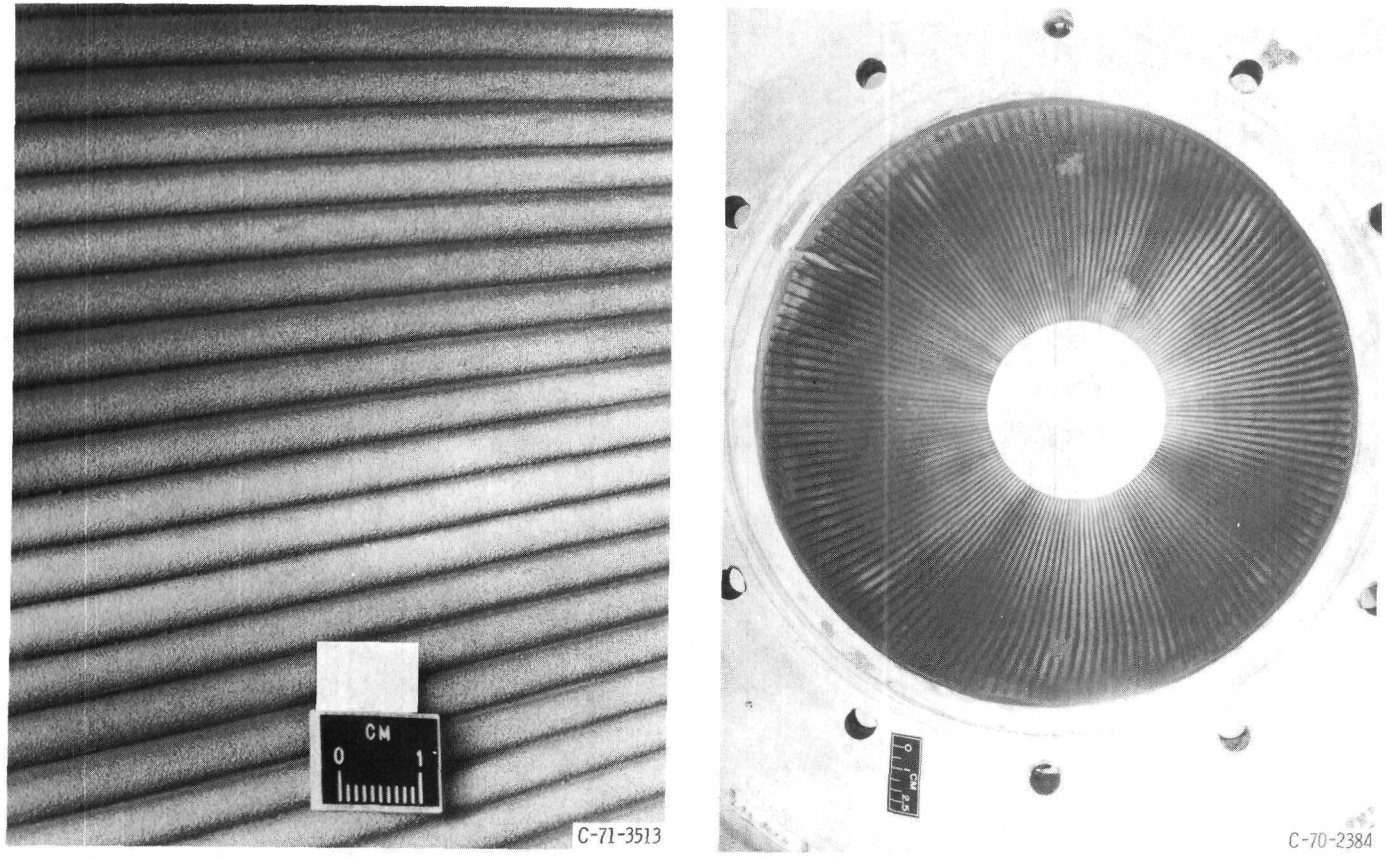

(a) Chamber.

Figure 7. - Thrust chamber 9 after runs.

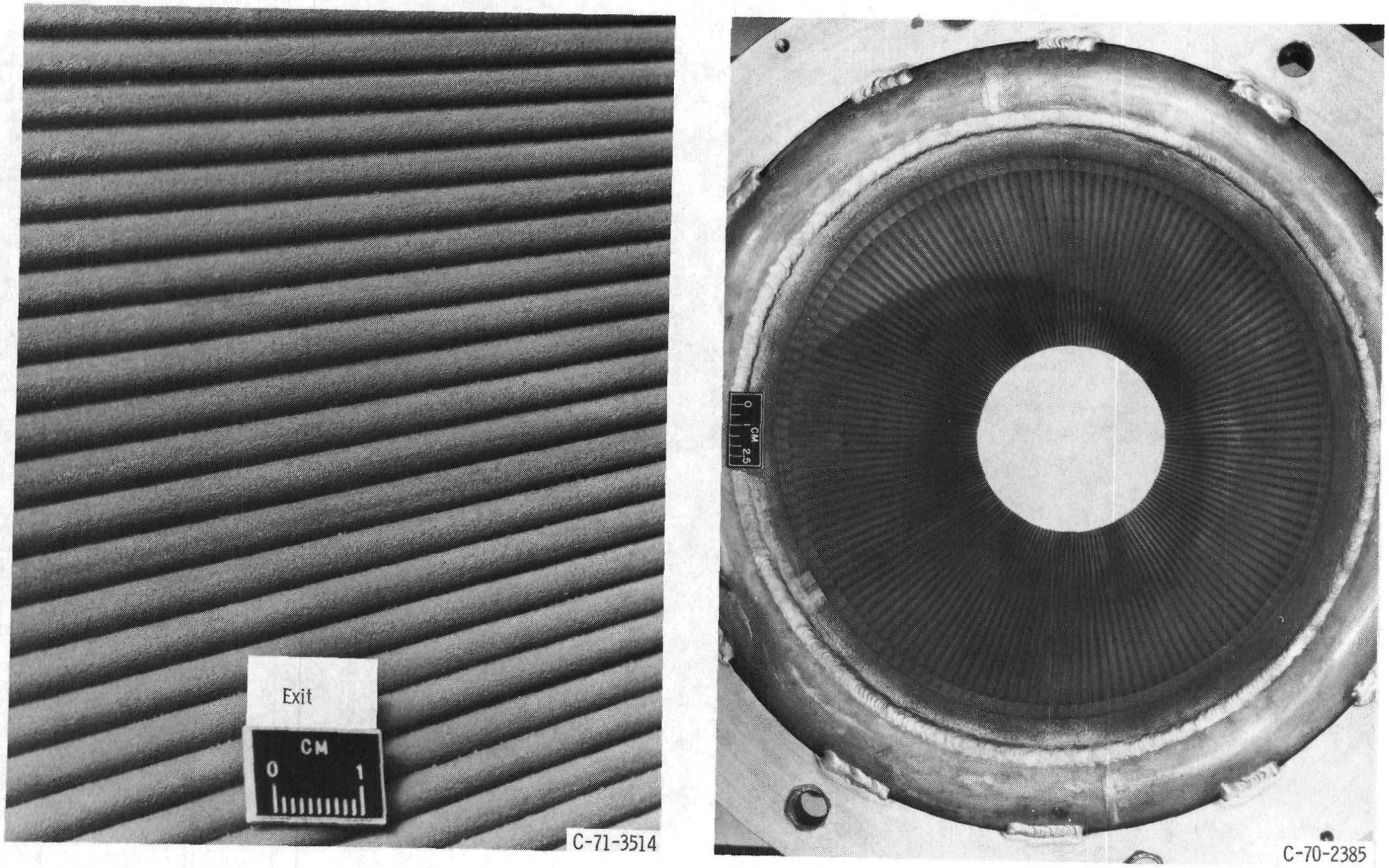

(b) Nozzle.

Figure 7. - Concluded.

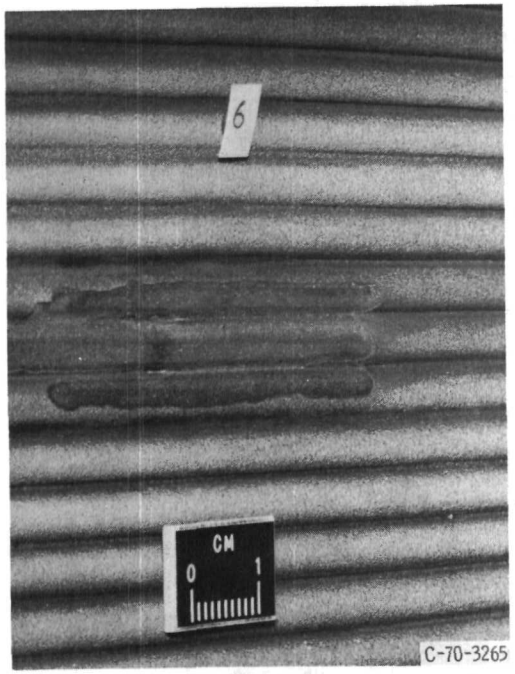

Figure 8. - Station 6 of thrust chamber 9, showing where the coating spalled from the instrument location.

Run	Approximate running time, sec	Chamber pressure, P_{ch}		Hydrogen content, percent
		MN/m^2	psia	
6	10	2.07	300	25
7	19	↓	↓	15
8	29			↓
9	38			
10	48			
11	57			
12	67	↓	↓	25
13	76	2.41	350	15
14	87	2.76	400	↓
15	96	3.10	450	
16	105	3.10	450	
17	115	2.07	300	

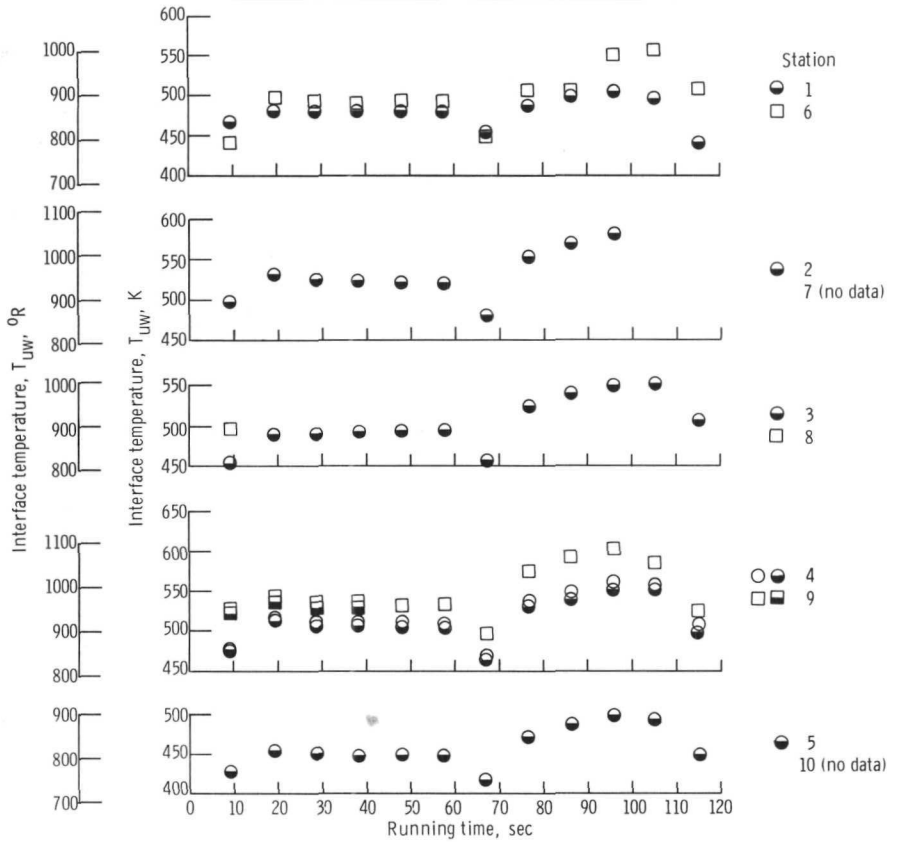

Figure 9. - Time history of interface temperature between metal wall and type 2 coating on thrust chamber 8 for various operating conditions.

Run	Approximate running time, sec	Chamber pressure, P_{ch}		Hydrogen content, percent
		MN/m^2	psia	
6	10	2.07	300	25
7	19			15
8	29			
9	38			
10	48			
11	57			
12	67			25
13	76	2.41	350	15
14	87	2.76	400	
15	96	3.10	450	
16	105	3.10	450	
17	115	2.07	300	

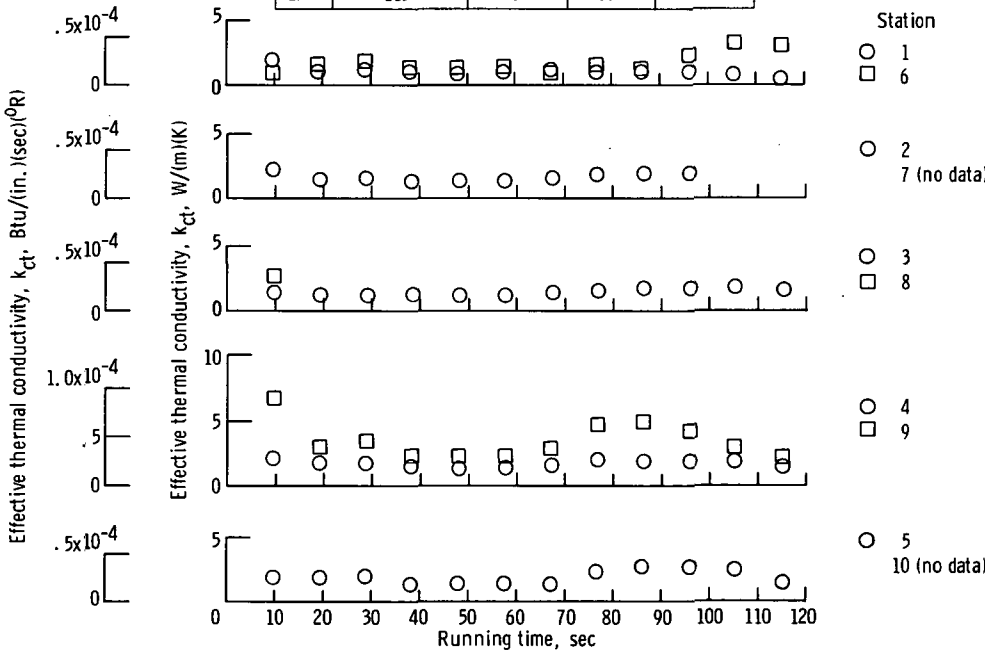

Figure 10. - Summary of effective thermal conductivity of type 2 coating in thrust chamber 8.

Run	Approximate running time, sec	Chamber pressure, P_{ch}		Hydrogen content, percent
		MN/m^2	psia	
28	10	2.07	300	15
29	20	2.07	300	
30	30	3.10	450	
31	40	3.10	450	
33	50	4.14	600	
34	60			
35	70			
36-37	80			
38	90			
39	100			
40	110			
41-42	120			
60	150			
61	180			
62	210			

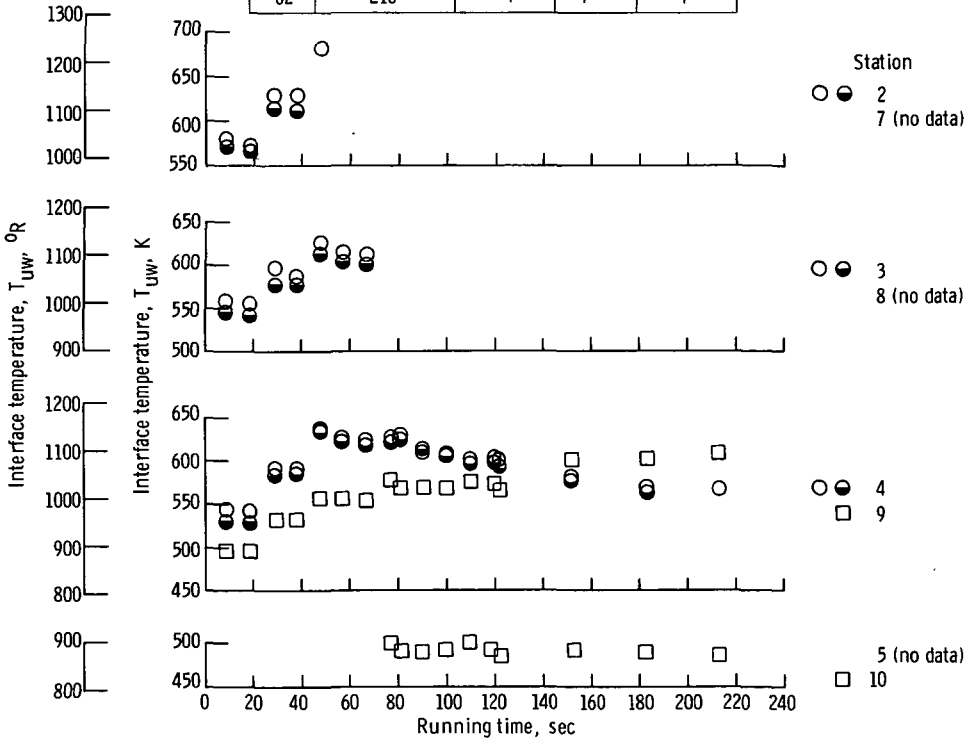

Figure 11. - Time history of interface temperature between metal wall and type 2 coating on thrust chamber 9 for various operating conditions. No data at station 1-6.

Run	Approximate running time, sec	Chamber pressure, P_{ch}		Hydrogen content, percent
		MN/m^2	psia	
28	10	2.07	300	15
29	20	2.07	300	
30	30	3.10	450	
31	40	3.10	450	
33	50	4.14	600	
34	60			
35	70			
36-37	80			
38	90			
39	100			
40	110			
41-42	120			
60	150			
61	180			
62	210			

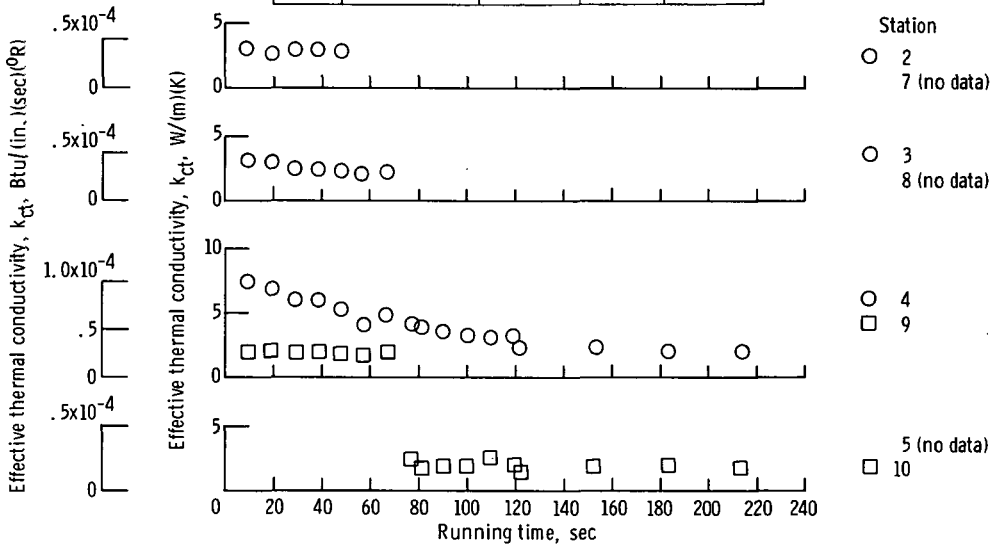

Figure 12. - Summary of effective thermal conductivity of type 2 coating on thrust chamber 9. No data at station 1-6.

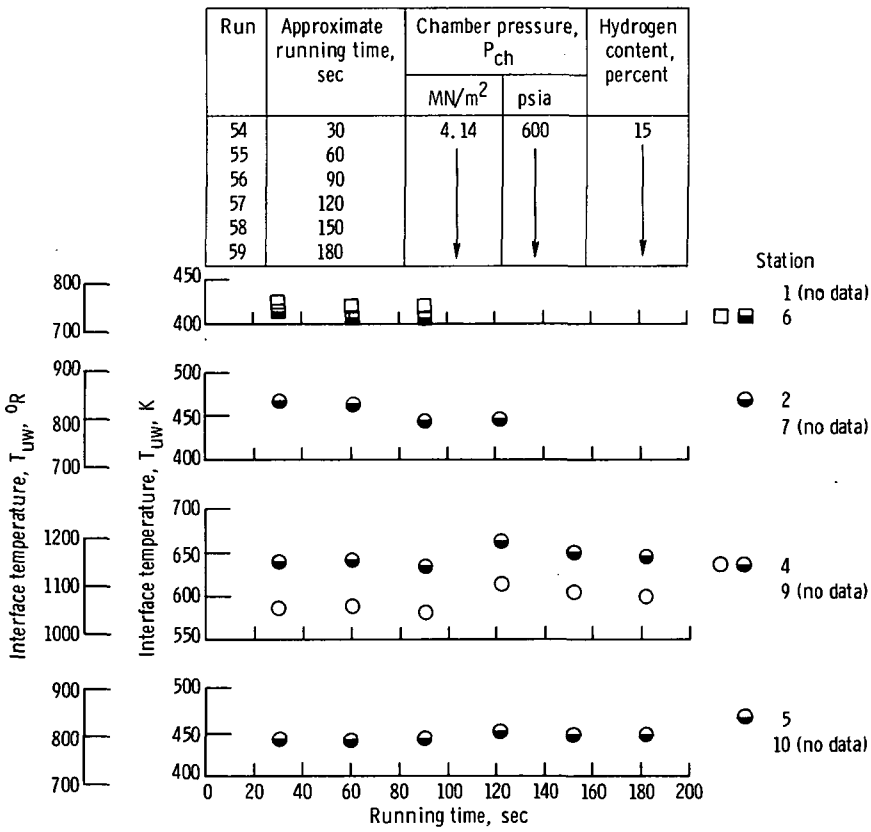

Figure 13. - Time history of interface temperature between metal wall and type 3 coating on thrust chamber 8. No data at station 3-8.

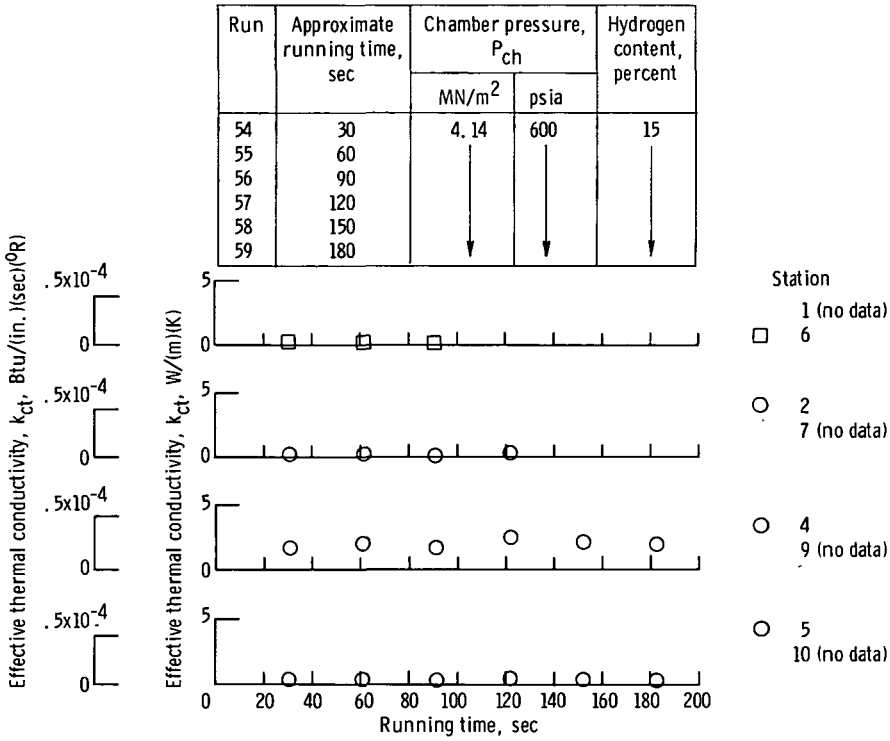

Figure 14. - Summary of effective thermal conductivity of type 3 coating on thrust chamber 8. No data at station 3-8.

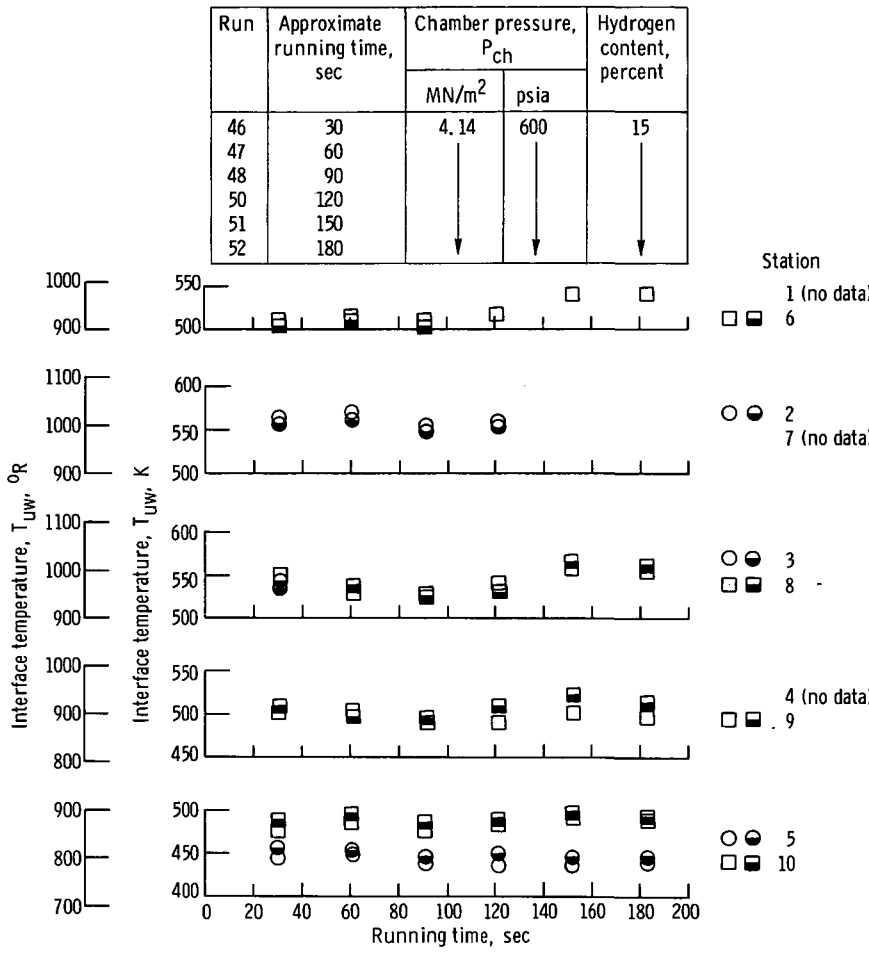

Figure 15. - Time history of interface temperature between metal wall and type 5 coating on thrust chamber 5.

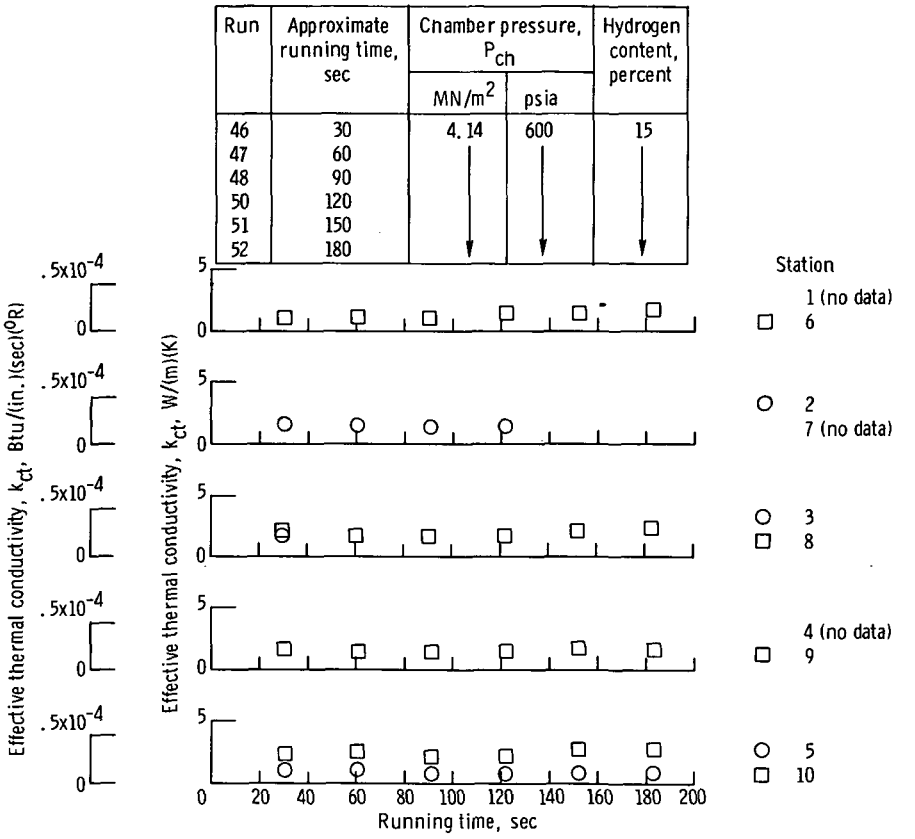

Figure 16. - Summary of effective thermal conductivity of type 5 coating on thrust chamber 5.

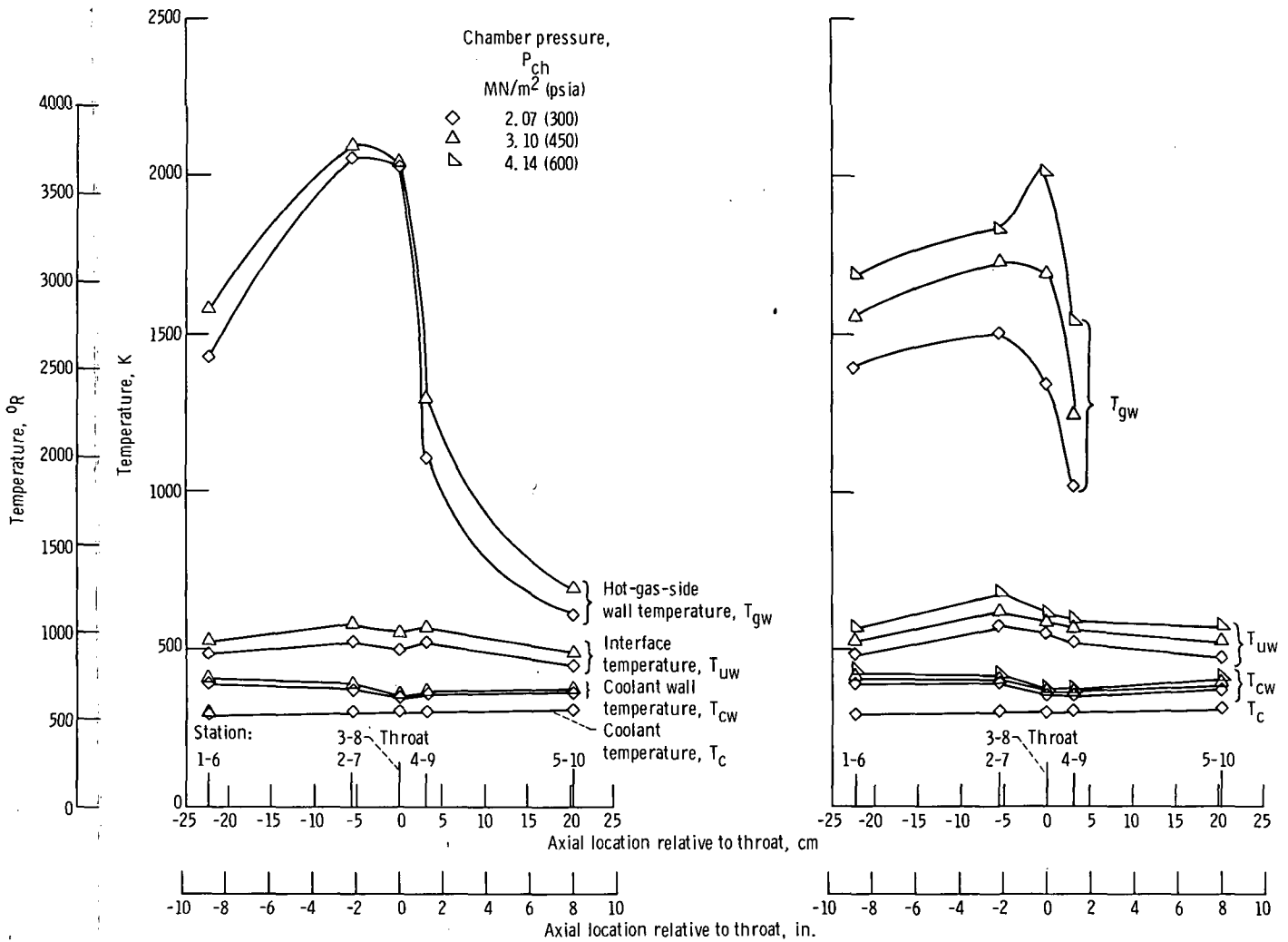

(a) Thrust chamber 8.

(b) Thrust chamber 9.

Figure 17. - Temperatures profiles determined from averaged interface and coolant temperatures for coating type 2 on thrust chambers 8 and 9. Hydrogen content, 15 percent (O/F of 5.67).

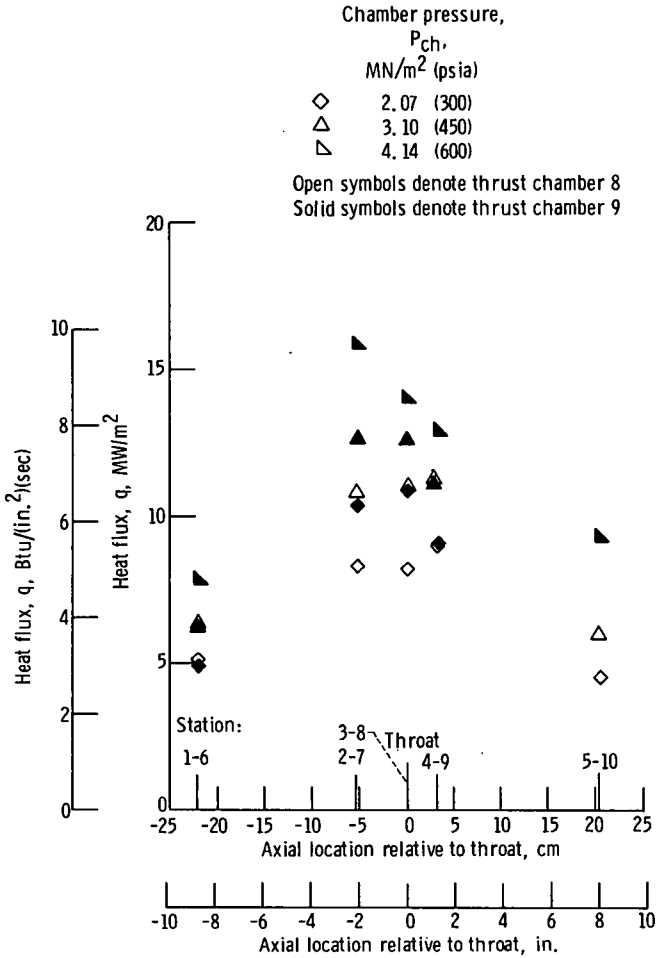

Figure 18. - Heat flux profile determined from averaged measured data for type 2 coating.

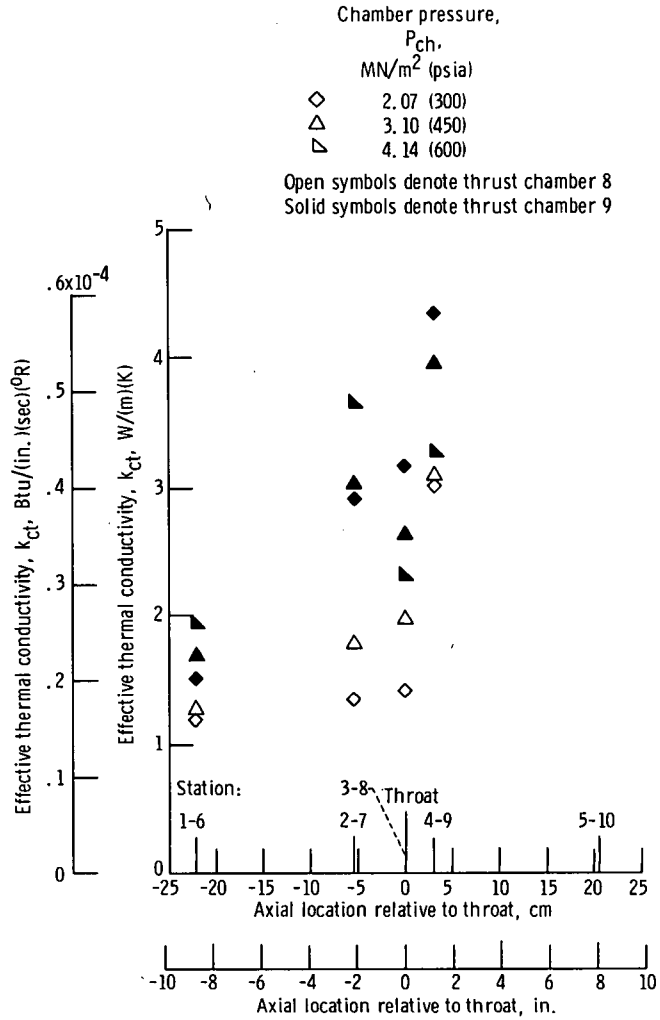

Figure 19. - Type 2 coating effective thermal conductivity determined from average measured data. Hydrogen content, 15 percent (O/F of 5.67).

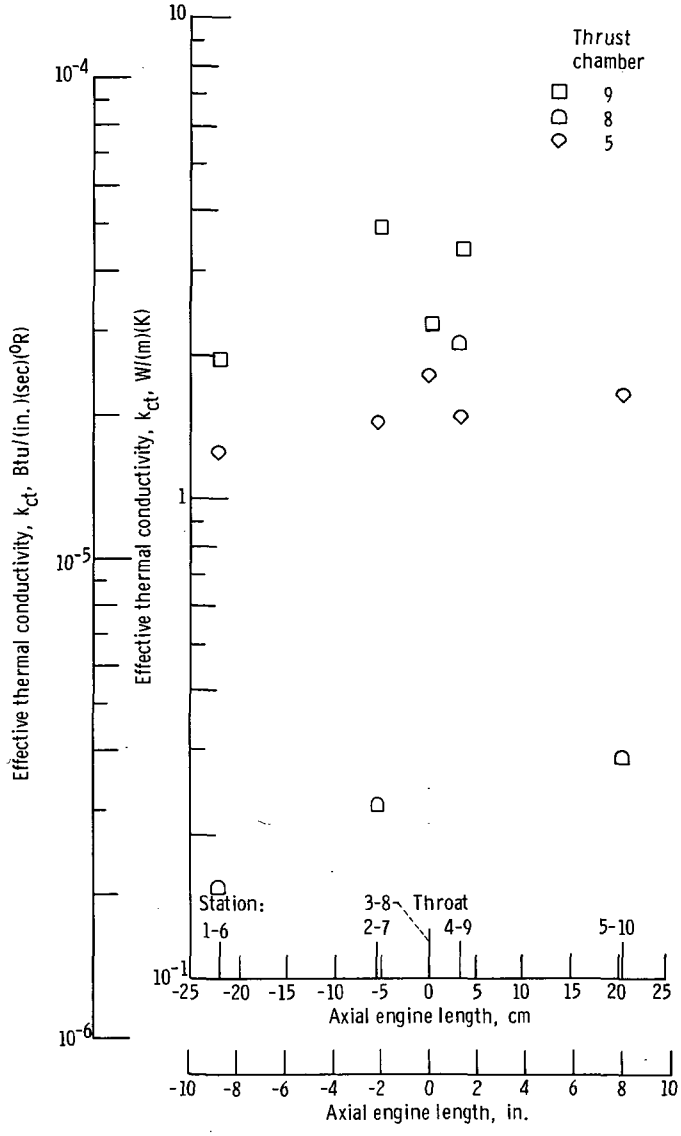

Figure 20. - Effect of changing coating material on effective thermal conductivity determined from averaged measured data. Chamber pressure, 4.14 MN/m^2 (600 psia).

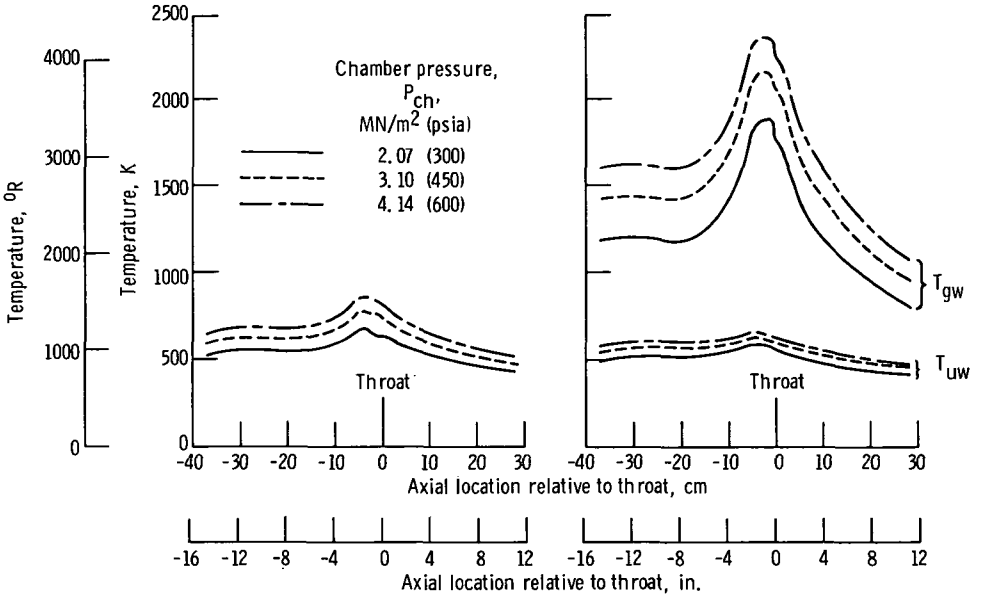

(a) Uncoated. Hot-gas-side wall temperature equal to interface temperature, $T_{gw} = T_{uw}$.

(b) Coated. Thickness, 0.0254 centimeter (0.010 in.); thermal conductivity, 2.242 W/(m)(K)(0.3x10^{-4} Btu/(in.)(sec)(°R).

Figure 21. - Theoretical wall temperature profiles.

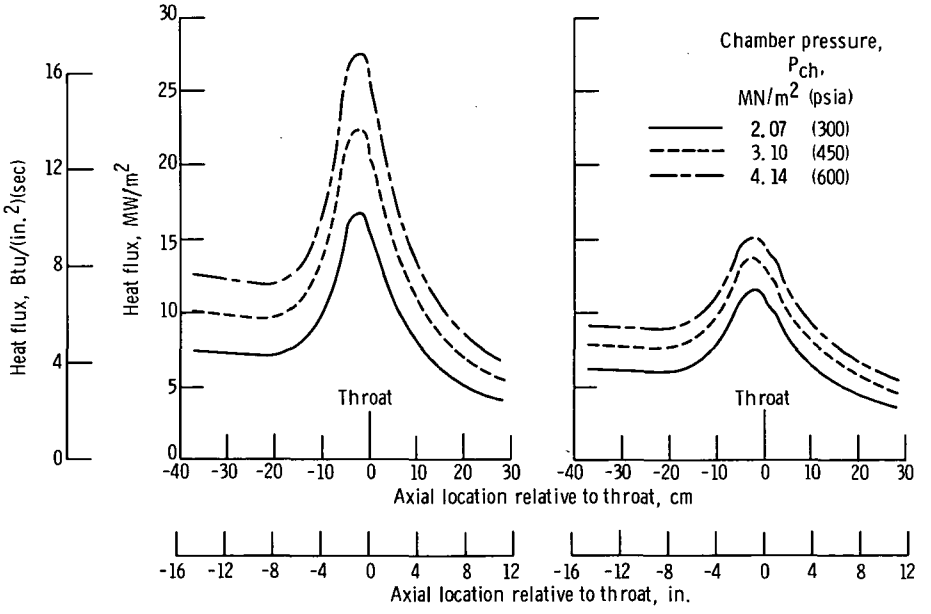

(a) Uncoated.

(b) Coated. Thickness, 0.0254 centimeter (0.010 in.); thermal conductivity, 2.242 W/(m)(K)(0.3x10^{-4} Btu/(in.)(sec)(°R)).

Figure 22. - Theoretical heat flux profiles.

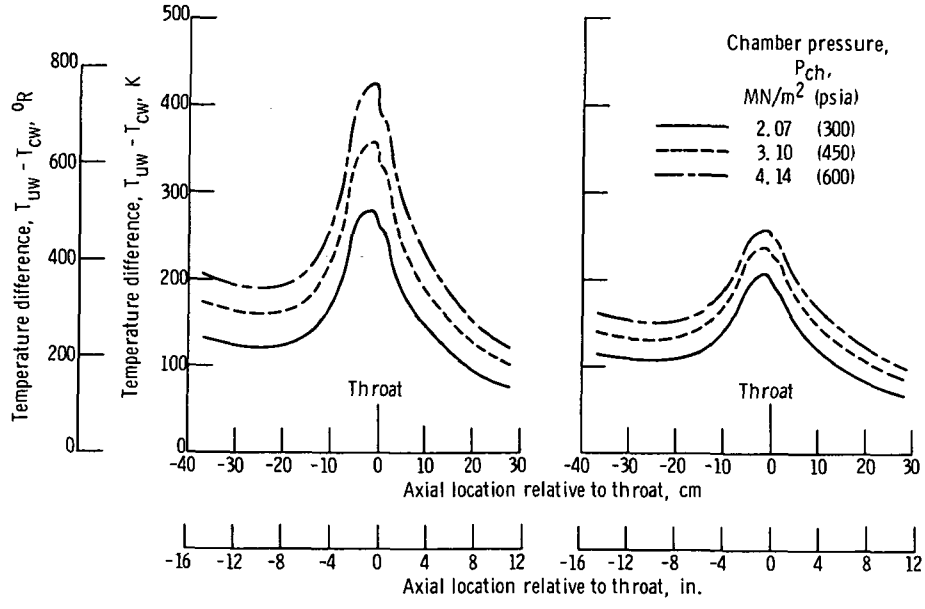

(a) Uncoated. (b) Coated.

Figure 23. - Theoretical temperature difference across metal wall.

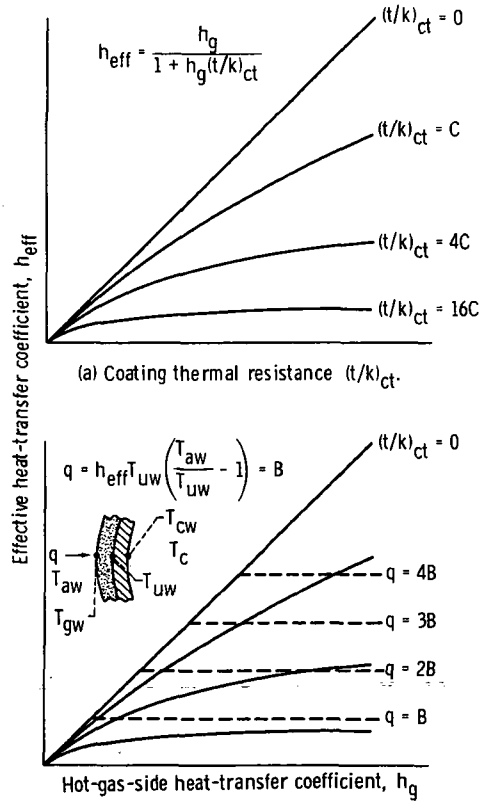

(a) Coating thermal resistance $(t/k)_{ct}$.

(b) Coating thermal resistance $(t/k)_{ct}$ and heat flux q.

Figure 24. - Graphical coating analysis.

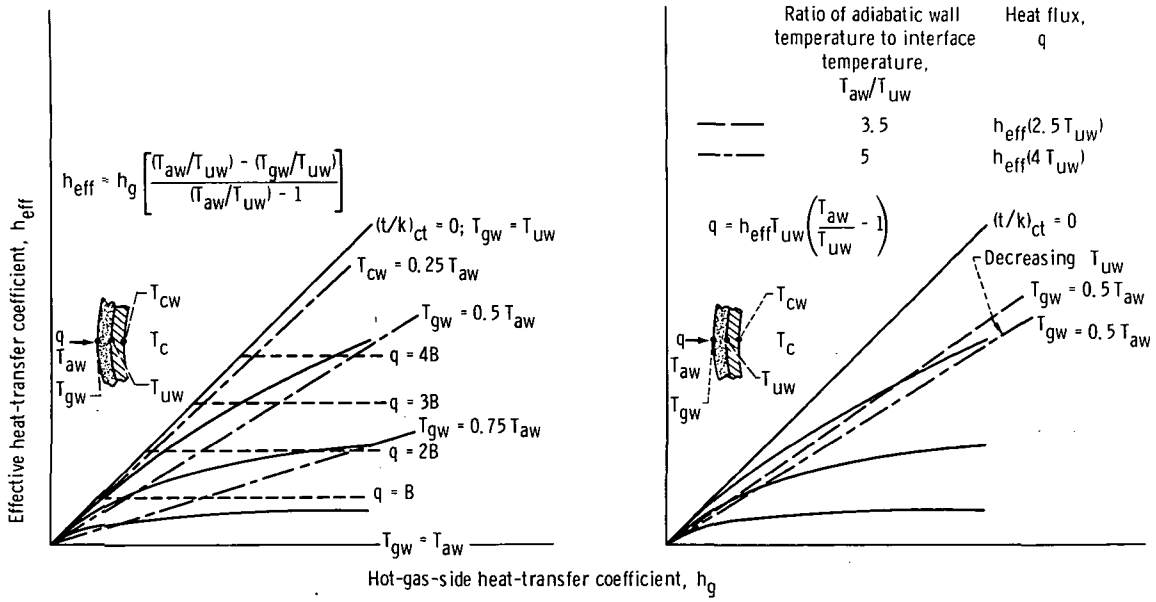

(c) Coating thermal resistance $(t/k)_{ct}$, heat flux q, and gas-side wall temperature T_{gw} as function of adiabatic wall temperature T_{aw}.

(d) Coating thermal resistance $(t/k)_{ct}$ and gas-side wall temperature T_{gw} as function of a variable interface temperature T_{uw}.

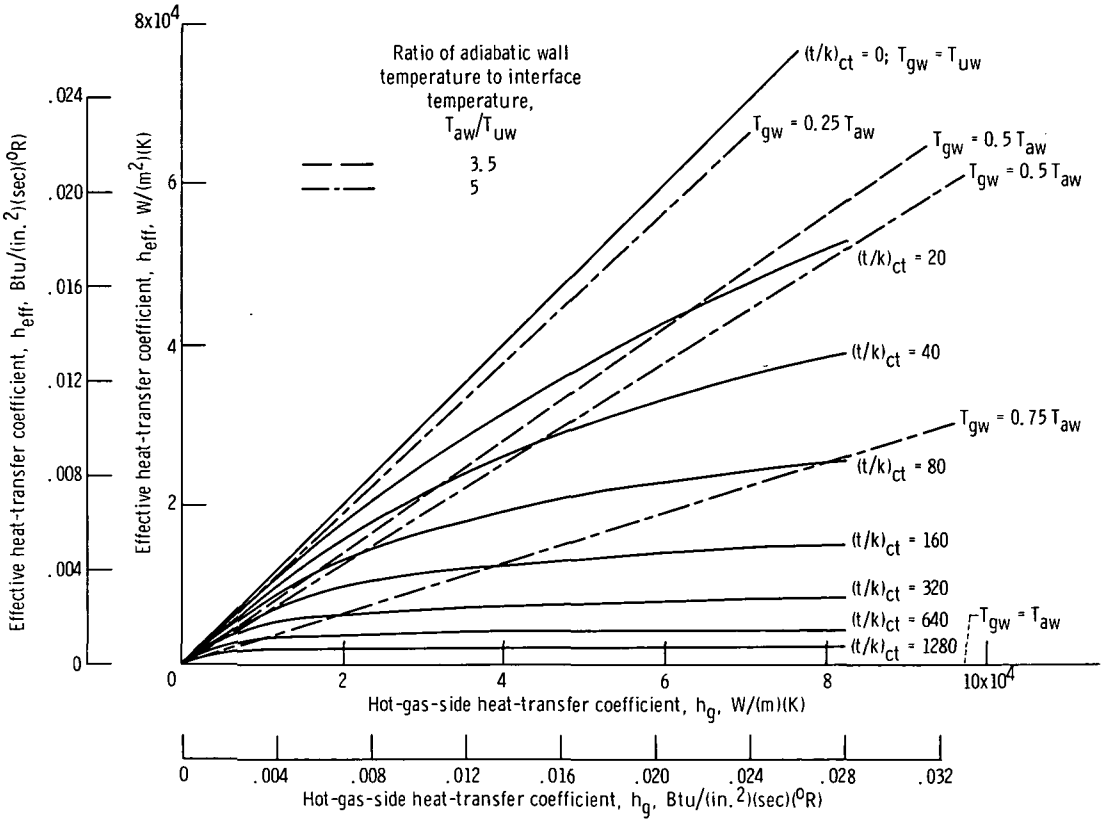

(e) Numerical clarification of parameters presented in figure 24(d).

Figure 24. - Concluded.

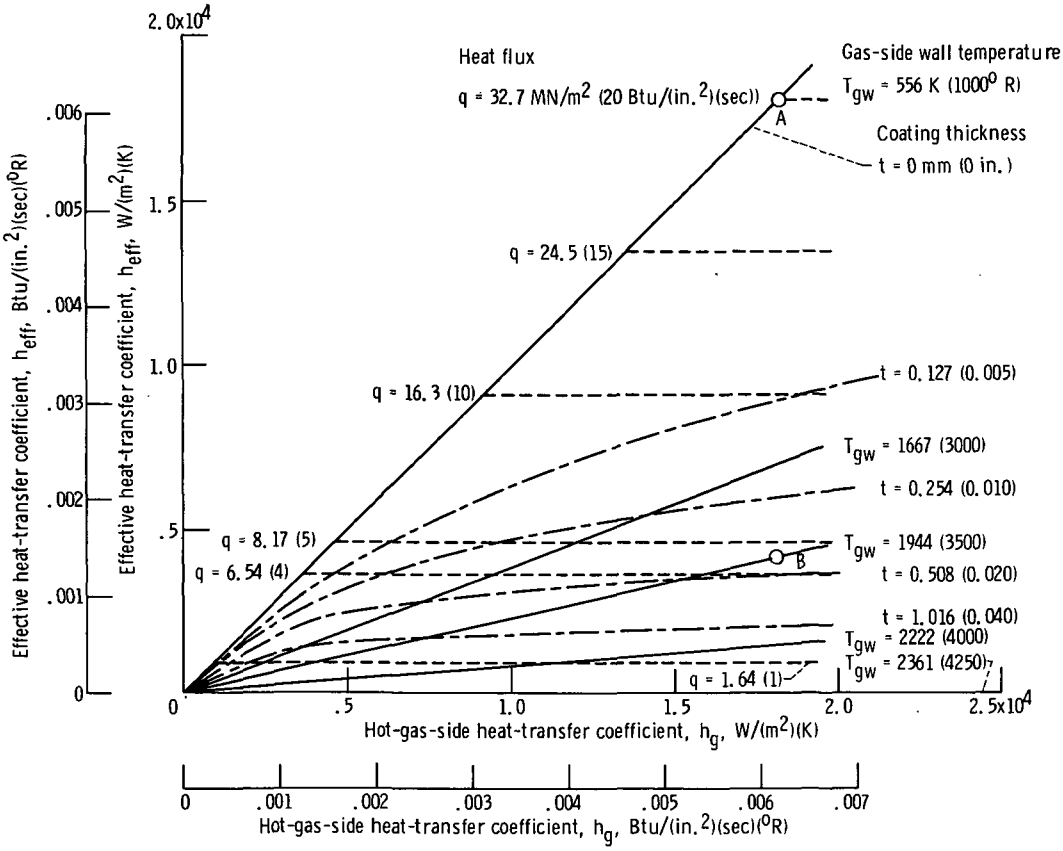

Figure 25. - Coating thickness analysis for conditions representative of a nuclear nozzle design: effective thermal conductivity, k_{ct}, 2.242 W/(m)(K) (0.3x10^{-4} Btu/(in.)(sec)(^{0}R)); adiabatic wall temperature, T_{aw}, 2361 K (4250^{0} R); interface temperature, T_{uw}, 556 K (1000^{0} R).

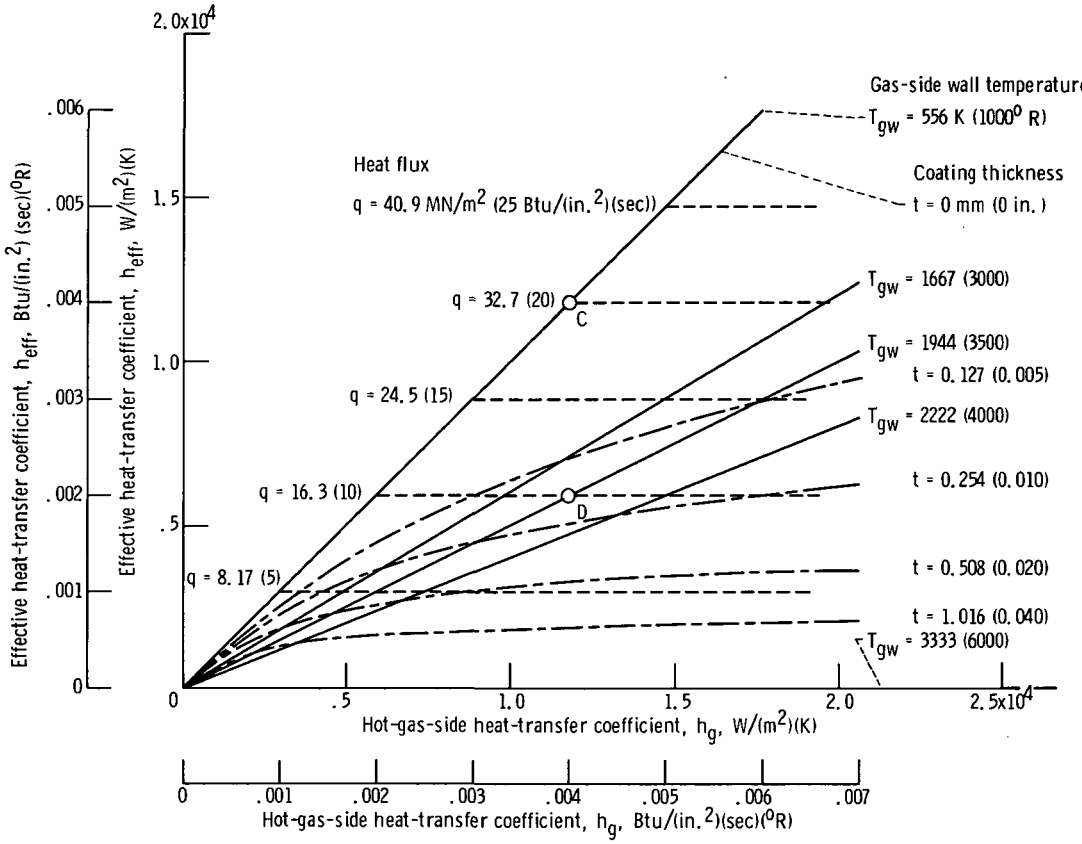

Figure 26. - Coating thickness analysis for conditions representative of a chemical rocket with low chamber pressure: effective thermal conductivity, k_{ct}, 2.42 W/(m)(K) (0.3x10^{-4} Btu/(in.)(sec)(°R)); adiabatic wall temperature, T_{aw}, 3333 K (6000° R); interface temperature, T_{uw}, 556 K (1000° R).

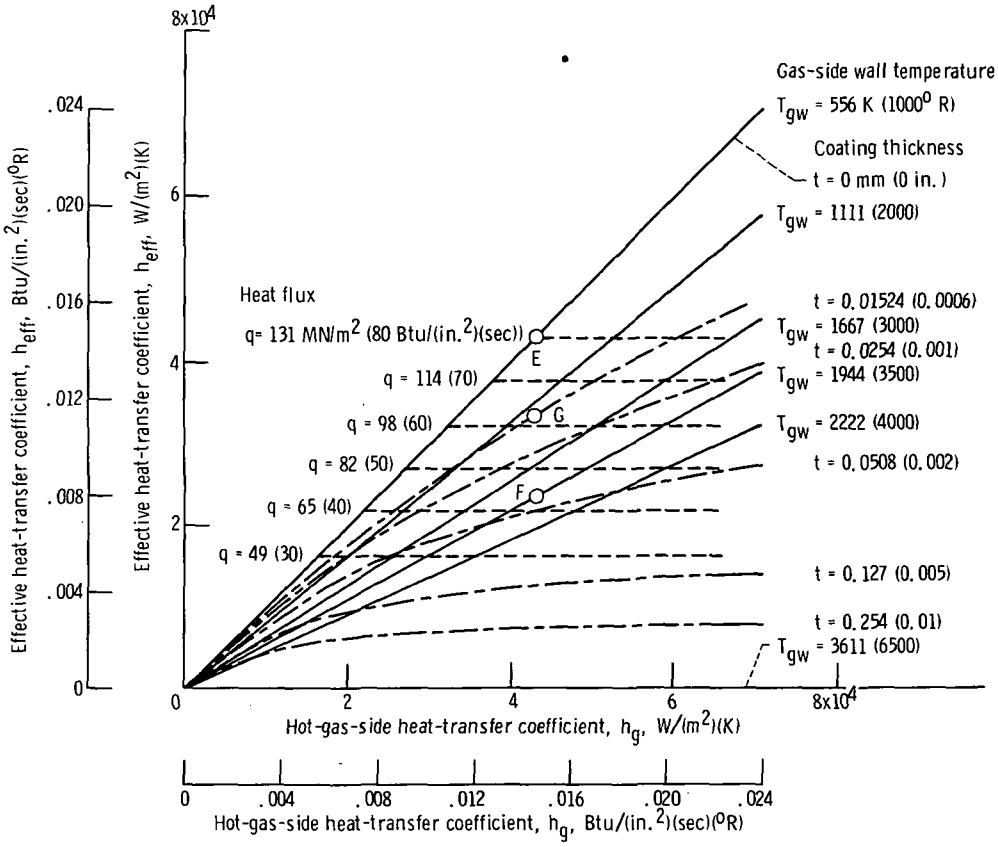

Figure 27. - Coating thickness analysis for conditions representative of a chemical rocket with high chamber pressure: effective thermal conductivity, k_{ct}, 2.242 W/(m)(K) (0.3x10^{-4} Btu/(in.)(sec)(°R)); adiabatic wall temperature, T_{aw}, 3611 K (6500° R); interface temperature, T_{uw}, 556 K (1000° R).

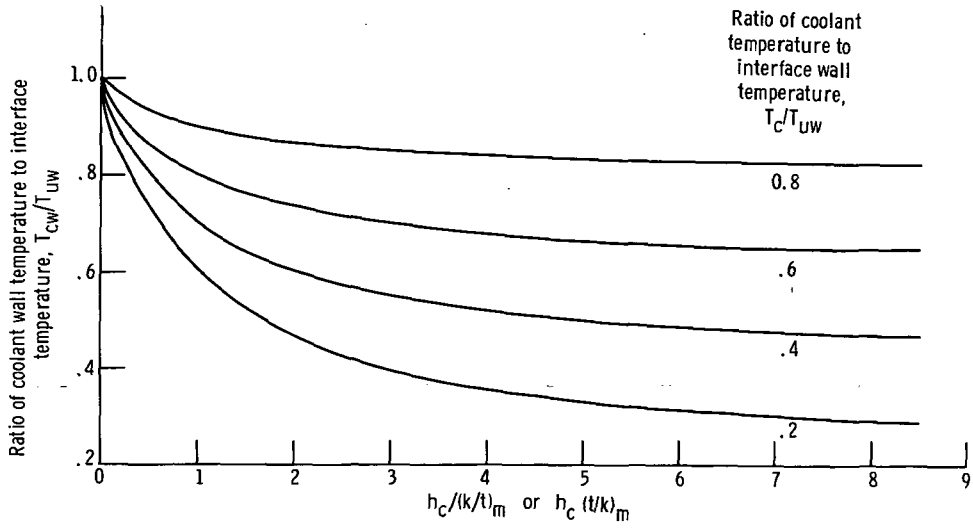

Figure 28. - Sensitivity of heat-transfer parameters on coolant side of thrust chamber.

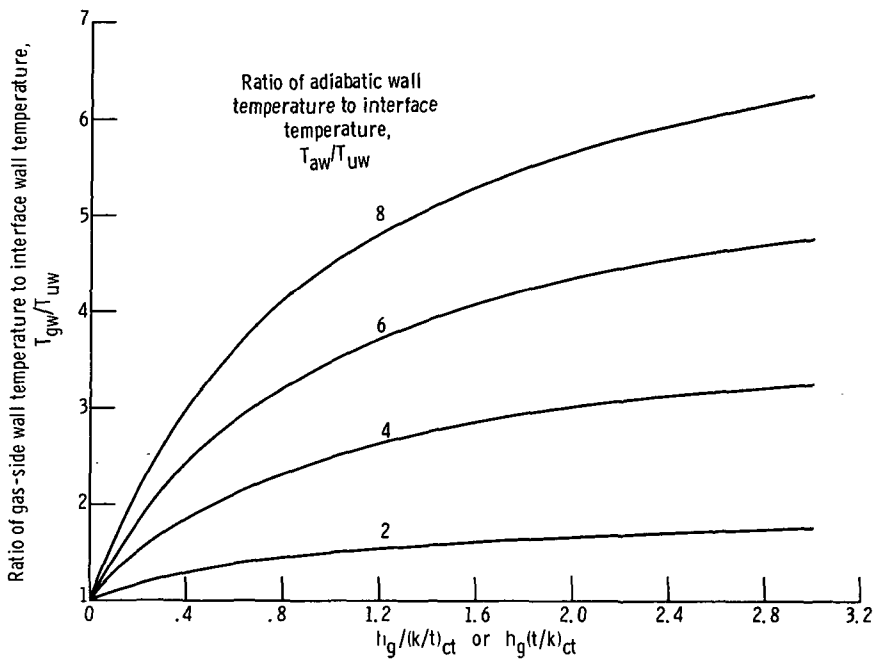

Figure 29. - Sensitivity of heat-transfer parameters on hot-gas side of thrust chamber.

NATIONAL AERONAUTICS AND SPACE ADMINISTRATION
WASHINGTON, D.C. 20546

OFFICIAL BUSINESS
PENALTY FOR PRIVATE USE $300

SPECIAL FOURTH-CLASS RATE BOOK

POSTAGE AND FEES PAID
NATIONAL AERONAUTICS AND SPACE ADMINISTRATION
451

U.S.MAIL

POSTMASTER: If Undeliverable (Section 158 Postal Manual) Do Not Return

"The aeronautical and space activities of the United States shall be conducted so as to contribute . . . to the expansion of human knowledge of phenomena in the atmosphere and space. The Administration shall provide for the widest practicable and appropriate dissemination of information concerning its activities and the results thereof."

—NATIONAL AERONAUTICS AND SPACE ACT OF 1958

NASA SCIENTIFIC AND TECHNICAL PUBLICATIONS

TECHNICAL REPORTS: Scientific and technical information considered important, complete, and a lasting contribution to existing knowledge.

TECHNICAL NOTES: Information less broad in scope but nevertheless of importance as a contribution to existing knowledge.

TECHNICAL MEMORANDUMS: Information receiving limited distribution because of preliminary data, security classification, or other reasons. Also includes conference proceedings with either limited or unlimited distribution.

CONTRACTOR REPORTS: Scientific and technical information generated under a NASA contract or grant and considered an important contribution to existing knowledge.

TECHNICAL TRANSLATIONS: Information published in a foreign language considered to merit NASA distribution in English.

SPECIAL PUBLICATIONS: Information derived from or of value to NASA activities. Publications include final reports of major projects, monographs, data compilations, handbooks, sourcebooks, and special bibliographies.

TECHNOLOGY UTILIZATION PUBLICATIONS: Information on technology used by NASA that may be of particular interest in commercial and other non-aerospace applications. Publications include Tech Briefs, Technology Utilization Reports and Technology Surveys.

Details on the availability of these publications may be obtained from:

SCIENTIFIC AND TECHNICAL INFORMATION OFFICE

NATIONAL AERONAUTICS AND SPACE ADMINISTRATION

Washington, D.C. 20546